Major and trace element emission rates in hydrothermal plumes in a tropical environment. The case of La Soufrière de Guadeloupe volcano

Manuel Inostroza, Séverine Moune, Roberto Moretti, Pierre Burckel, Elodie Chilin-Eusebe, Celine Dessert, Vincent Robert, Caroline Gorge

Major and trace element emission rates in hydrothermal plumes in a tropical environment. The case of La Soufrière de Guadeloupe volcano

Manuel Inostroza[1,2,3], Séverine Moune[1,2,4], Roberto Moretti[1,2], Pierre Burckel[1], Elodie Chilin-Eusebe[1,2], Celine Dessert[1], Vincent Robert[5], Caroline Gorge[1]

[1]Université de Paris Cité, Institut de Physique du Globe de Paris, UMR 7154 CNRS, F75005, Paris, France

[2]Observatoire Volcanologique et Sismologique de Guadeloupe, Institut de Physique du Globe de Paris, F97113, Gourbeyre, France.

[3]Millennium Institute on Volcanic Risk Research - Ckelar Volcanoes, F1249004, Antofagasta, Chile.

[4]CNRS, IRD, OPCG Laboratoire Magmas et Volcans, Université Clermont Auvergne, F63000, Clermont-Ferrand, France

[5]IRD, IMAGO LAMA, F98800 Nouméa, France

*Corresponding Author: manuelinostrozap@gmail.com; https://orcid.org/0000-0003-0800-3508

Keywords: trace elements, filter packs, emission rates, volcanic-hydrothermal system, La Soufrière de Guadeloupe, pollution

ABSTRACT

Hydrothermal or low-temperature volcanic emissions, most commonly occurring in fumarolic environments, dominate the global volcanic landscape. This work presents physicochemical characterization of the aerosols contained in steam- and H_2S-rich plumes discharged from La Soufrière volcano, in conjunction with the first report on their heavy metal degassing emission rates. Our results indicate that the plume is enriched in certain lithophile (K, Ti, Si, Al, Mn, and Mg) and siderophile (Fe) elements, related to hydrothermal rock leaching, and chalcophile (Sb, As, Zn, Pb, and Tl) elements, which are usually degassed from the magma source. Heavy metal emission rates were found to be below 15 g/d, which are modest compared to available worldwide data. Nevertheless, Cr and Sb emission rates were very similar to those of Lascar volcano (Chile), which instead has produced magmatic eruptions in recent times. We propose that the depth of the magma chamber and the input of meteoric waters play an important role in scavenging heavy metals in the hydrothermal system of magmatic-hydrothermal volcanoes. Notwithstanding low heavy metal emission rates, La Soufrière can be regarded as an important pollution source in the Lesser Antilles volcanic arc.

1 INTRODUCTION

Surficial volcanic gas emissions indicate the presence of magma chambers evolving in shallower crustal levels and are composed of gases (H_2O, CO_2, SO_2, H_2S, and HCl) and aerosols containing lithophile, siderophile, and chalcophile elements. These can be classified into magmatic and hydrothermal emissions

according to their chemical compositions, outlet gas temperatures, and the degree of interaction with host rocks and aquifers hosted in the volcanic edifice (e.g., Giggenbach, 1996; Symonds et al., 2001; Fischer and Chiodini, 2015; Moretti and Stefánsson, 2020). Typical magmatic emissions are characterized by significant concentrations of SO_2 and halides, high outlet gas temperatures (>450 °C; Aiuppa et al. 2017), and minimal scrubbing processes (Symonds et al. 2001). On the other hand, hydrothermal emissions are enriched in H_2S and present lower gas temperatures (<250 °C), suggesting water-rock interactions within a hot water reservoir supplemented with heat and acid fluids from magma underneath. Furthermore, hydrothermal emissions with substantial magmatic influence and intermediate temperatures (250-450 °C) are usually called magmatic-hydrothermal emissions (e.g., Aiuppa et al. 2017).

Volcanic emissions represent one of the primary trace element sources into the atmosphere, supplying more than 100 kg/day of certain metals and metaloids (e.g., B, As, Cu, Zn, Tl, Pb, among others; e.g., Mather et al. 2003; Moune et al. 2010; Calabrese et al. 2011; Mather 2015; Mandon et al. 2019). These elements include so-called heavy metals, which are toxic even at low concentrations and are degassed as chlorides, sulfates, sulfides, or directly as metals (e.g., Moune et al. 2010; Bagnato et al. 2015; Scholtysik and Canil, 2020). Moreover, heavy metals are frequently associated with bioaccumulation in terrestrial and aquatic environments, which then enter the food chain and drinkable water, impacting human health in the surrounding communities (e.g., Varrica et al. 2014; Vigneri et al. 2017; Tomašek et al. 2022). Though previous trace element studies have investigated the magmatic emissions (e.g., Crowe et al. 1987; Africano et al. 2002; Aiuppa et al. 2003; Zelenski et al. 2013), hydrothermal fumarolic emissions remain less studied (e.g., Chen et al. 2005; Mandon et al. 2019) primarily because low-temperature and low-flux emissions contain lesser amounts of metals than magmatic emissions, and are more difficult to be characterized. Furthermore, they result from a more complex history in terms of water-rock interaction, that involves numerous physicochemical processes that are known but hard to quantify. These processes, including gas phase condensation, leaching from host rocks, precipitation of secondary mineral phases, and brine evaporation (Africano and Bernard 2000), can scavenge some or add other trace elements. In accordance with these processes, unemitted trace elements potentially form ore deposits (Blundy et al. 2021). Consequently, hydrothermal emissions are generally less enriched in volatile trace elements and include greater concentrations of rock-forming elements (e.g., Symonds et al. 1990; Obenholzner et al. 2003; Inostroza et al. 2022a,b).

La Soufrière de Guadeloupe (hereafter La Soufrière) is an andesitic volcano in the Lesser Antilles arc, formed by the subduction of the Atlantic Plate below the Caribbean Plate (Feuillet et al. 2002). La Soufrière has presented persistent degassing since 1992, which gradually increased in intensity in the last three decades. Currently, fumarolic emissions here are characterized by high amounts of steam (~200 t/d), CO_2 (3-15 t/d), H_2S (0.6-4.0 t/d; Allard et al. 2014; Tamburello et al. 2019; Moune et al. 2022), and low outlet gas temperatures (up to 111 °C on March 23, 2018; Moretti et al. 2020a). Recently, Inostroza et al. (2022a,b) demonstrated that condensed gases collected directly at the vent contained significant amounts

of lithophile and chalcophile elements, along with heavy metals such as Sb, Bi, and Zn. However, the behavior and enrichment of these elements in low-temperature plumes are still poorly constrained.

This work combines filter pack and MultiGas data collected from low-temperature volcanic plumes at La Soufrière volcano to, i) constrain the physicochemical characteristics of gas and aerosol phases, ii) determine their major and trace element enrichments, and iii) determine heavy metal emission rates degassed from the volcano. This study builds on the previous findings of Inostroza et al. (2022a,b) and their interpretations on major and trace element concentrations in condensed gases, in addition to elemental behavior according to variations in hydrothermal activity. Further, it contributes to the first trace element emission rates in La Soufrière, and as per our knowledge, is one of the first records considering low-temperature (~95 °C) volcanic emissions.

2 GEOLOGICAL SETTING AND HYDROTHERMAL ACTIVITY

La Soufrière volcano (16.0446 °N, 61.6642 °W, 1467 m.a.s.l.) belongs to the Grande Découverte Volcanic Complex (Fig. 1) and is the highest point in the Lesser Antilles Arc (Komorowski et al. 2005). La Soufrière edifice was developed in the last 11500 years BP (Komorowski et al. 2005; Boudon et al. 2008), after recurrent magmatic and non-magmatic eruptions. The last magmatic eruptions (Vulcanian, VEI 2-3) occurred in 1530 and 1657 CE (Legendre 2012; Metcalfe et al. 2021) and were followed by intermittent phreatic explosions in 1797-98, 1836-37, 1956, and 1976-77 (Legendre 2012; Hincks et al. 2014) which shaped the current fractured appearance of the summit lava dome emplaced in 1530.

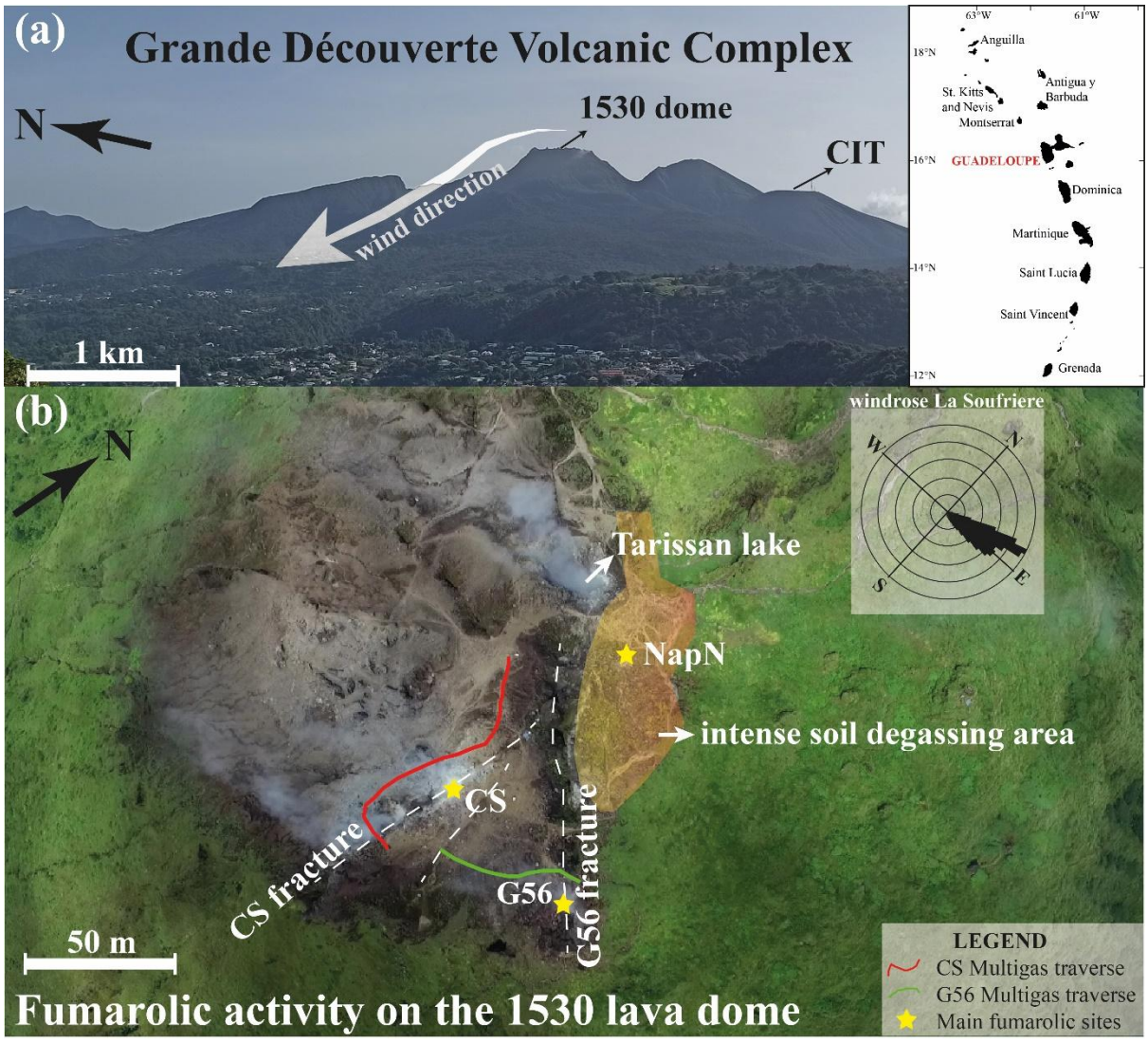

Figure 1. (a) Over view of La Grande Découverte Volcanic Complex and (b) An aerial photograph showing the volcano summit and hydrothermally altered zones (areas without vegetation), emphasizing the position of primary fumarolic emissions and fractures (white dash lines). Cratere Sud (CS), Gouffre 56 (G56), and Napoleon Nord (NapN) vents are situated along fractures and intense soil degassing areas. The wind direction and wind rose information were taken from 2016-2019 data collected by the Sanner weather station (property of the OVSG-IPGP, 16.04497 °N, 61.66272 °W, 1411 m.a.s.l.) and then treated by Rave et al. (In press). The Citerne (CIT), the place where the atmospheric background sample was collected, is also shown.

The La Soufrière summit presents vigorous fumarolic activity mainly along Cratère Sud (CS) and Gouffre 1956 (G56) fractures, with the soil degassing area progressively expanding to the NE (Fig. 1; Jessop et al. 2021). This activity is caused by the input of heat and gases from andesitic mush zones located 7-9 km below the summit (Pichavant et al. 2018; Metcalfe et al. 2021) and their subsequent interactions with the hydrothermal system, sustained by up to 6 m of rain per year (Dessert et al. 2015). This hydrothermal

system appears to be distributed from a few hundred meters up to ~2.5 km below the summit (Rosas-Carbajal et al. 2016; Moretti et al. 2020a) and plays a critical role in buffering deep magmatic fluids favoring their cooling, condensation, and reactions with surrounding rocks (Brombach et al. 2000; Salaün et al. 2011). Such effects have been noted at the summit area given the presence of the Tarissan acid lake, relatively stable outlet gas temperatures similar to saturated steam vapor at the pressure of the summit (~95 °C), and intense hydrothermal alteration (Salaün et al. 2011; Heap et al. 2021).

H_2S has been found to be the predominant sulfur species (0.3-0.6 mol%) in fumarolic emissions at La Soufrière; SO_2 has only been detected through MultiGas measurements with common SO_2/H_2S ratios between 0.004 and 0.1 (Tamburello et al. 2019; Moune et al. 2022). Furthermore, HCl has been measured at concentrations of ~0.2 mol% (Villemant et al. 2014), which have shown notable increase since the early 2000s (Bernard et al. 2006; Allard et al. 2014; Inostroza et al. 2022b). Low outlet gas temperatures and the composition of discharged fluids measured by direct sampling and MultiGas suggest the presence of a hydrothermal-dominated system with shallow magmatic influence (Brombach et al. 2000; Villemant et al. 2014; Tamburello et al. 2019; Moretti et al. 2020a; Moune et al. 2022; Inostroza et al. 2022b). Recent studies have shown variable spatio temporal behavior in the numerous fumarolic emissions of La Soufrière; these have been attributed to the following: i) different interactions of deep magmatic gases with hydrothermal aquifers (Tamburello et al. 2019), ii) different degassing pathways, that is, fractures versus diffuse degassing (Rosas-Carbajal et al. 2016; Tamburello et al. 2019; Moune et al. 2022); and iii) compositional changes induced by external forces such as extended dry seasons (Moune et al. 2022). These studies suggest that G56 and CS (Fig. 1) are the fumarolic sites with substantial "magmatic" contributions. In contrast, emissions from the Napoleon Nord (NapN) and the entire northeastern summit area of the dome appear to be strongly affected by scrubbing processes, also occurring at a very late stage by interactions with local shallow groundwaters (Tamburello et al. 2019; Inostroza et al. 2022a). Continuous monitoring at CS allowed identification of considerable temperature and compositional changes. These fluctuations suggest that CS could be connected with a deeper portion of the hydrothermal system, particularly sensitive to internal (input of magmatic gases and heat) and external (input of meteoric water or changes in the host-rock permeability) forces perturbing the hydrothermal reservoir(s) (Moretti et al. 2020a; de Bremond d'Ars and Gibert 2022; Moune et al. 2022).

Previous studies on gas condensates (Chen et al. 2014; Inostroza et al. 2022a) show that La Soufrière is an important emitter of major and trace elements. According to Inostroza et al. (2022a), most of those elements are dispersed as small rock-related solid fragments eroded from fumarolic conduits and tiny aqueous particles containing rock-related and deep-sourced metal/metalloid elements. Transport of tiny aqueous particles is favored by lower outlet gas temperature and more significant steam proportions in La Soufrière fumarolic gases compared to typical medium-high temperature volcanic emissions (Inostroza et al. 2022a). In general terms, gas condensates from NapN and CS show elevated S, Sb, B, Cl, Bi, Br, and Zn concentrations relative to andesitic host rocks (Inostroza et al. 2022a).

3 SAMPLING AND ANALYTICAL METHODS

3.1 Filter pack measurements

The filter pack is an active gas and particle filtration method common in atmospheric and volcanological studies, characterized by its lightweight, robust, and small sized instrumentation. In volcanology, this technique consists of the use of alkaline-impregnated filters to trap volcanic acid gases (SO_2, HCl, and HF) and polytetrafluoroethylene (PTFE) filters for aerosols (Crowe et al. 1987; Finnegan et al. 1989; Gauthier and Le Cloarec 1998; Allen et al. 2000). Given the predominance of H_2S compared to SO_2 in fumarolic emissions, this study used the modified sampling and analytical methods employed in Aiuppa et al. (2005) and described below.

Before field sampling, ashless paper filters (Wathman™ 1440-047) were impregnated with two solutions to independently trap gaseous SO_2 and H_2S. Gas filters dedicated to trapping SO_2 were impregnated with a solution of 1.2 M $NaHCO_3$, glycerol (10 wt.%), and methanol (40 wt.%) (Allen et al. 2000), while those for H_2S were impregnated with 1 M $AgNO_3$ (Sicardi 1955; Natusch et al. 1972; Aiuppa et al. 2005b), and glycerol (10 wt.%). Finally, PTFE (Fluoropore™ membrane FALP04700) and gas filters were carefully mounted inside a clean box using plastic tweezers.

Tests at La Soufrière volcano's fumarolic area allowed us to adapt the sampling method according to the high relative humidity (RH ranging from 80 to 100%, Table 1) and the steam- and H_2S-rich chemistry of fumarolic gases. These sampling tests helped us make two crucial decisions. First, more attention was paid to climatic conditions, trying to sample only in time intervals without rain or drizzle, and on days with less relative humidity to reduce possible leaching from the filters on the field. Second, it was noted that humidity could affect trapping efficiency on the first gas filter, causing the second gas filter to represent more than 10% of the gas. However, it was assumed that for a measurement to be valid, the last filter must contain negligible concentrations (<10%; Mioduszewski and Kress 2008). Subsequently, a third gas filter was included in the holder, ensuring complete entrapment of S-compounds (Fig. 2).

Sampling was done using three filter pack holders gathered in parallel (Figs. 2 and 3). Each holder (H_A, H_{SO2}, and H_{H2S}; Fig. 2) was assembled using a PTFE filter in front, while for H_{SO2} and H_{H2S}, three gas filters were assembled behind the PTFE filter. Air was drawn through the holders using three diaphragm pumps (one Charles Austen® Capex V2 and two Boxer® 3K) connected to 12 V portable batteries. Filtration of diluted volcanic plumes was carried out at flow rates of 0.72, 0.40, and 0.42 m^3/h (Table 1), sampling a volume ranging from 0.13 to 0.72 m^3. Flow rates were calibrated before sampling, showing errors of approximately 5%. H_A were exposed to the plume for longer times (60 min) to trap considerable amounts of particles, while H_{H2S} and H_{SO2} were exposed for 15 and 25 min, respectively, to avoid filter saturation.

The plume was sampled from three sites located at <10 m from the vent (3 and 5 m from CS and NapN, respectively, and ~10 m from the G56 vent; Table 1) and at 0.5-1.2 m above the soil (Fig. 3a, b) to reduce

the influence of the soil degassing and dust particles blown by the wind. After collection, aerosol and gas filters were stored in sealed plastic holders and left in the fridge. It was noted that $AgNO_3$-gas filters became brown because of their reaction with H_2S (Fig. 3e), as described by Aiuppa et al. (2005). Additionally, during and after sampling, presence of droplets caused by condensation of the gas phase and humidity were observed on PTFE filters, especially on the wettest days (Fig. 3b, 3d). Atmospheric background for aerosol and gases were collected at La Citerne (CIT; Fig. 1), situated 1400 m SE of the volcano (~1000 m a.s.l.) in an upwind site not affected by the volcanic plume dispersion (Fig. 1).

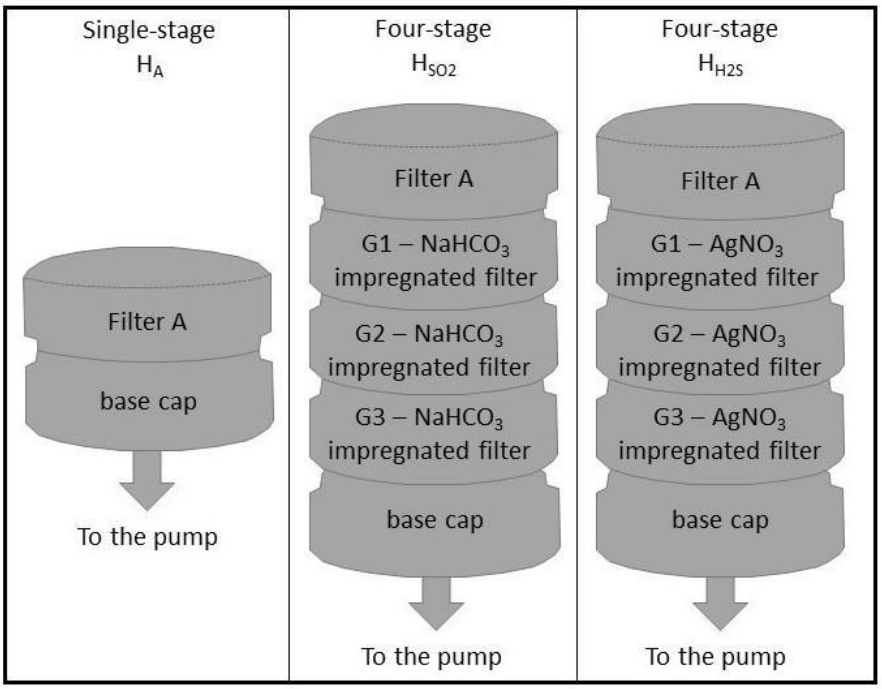

Figure 2 Sketch describing filter pack assemblage used for sampling volcanic plumes at La Soufrière volcano. At each site, three filter pack holders called H_A, H_{SO2}, and H_{H2S} were arranged to trap aerosols, aerosols+SO_2, and aerosol+H_2S, respectively. The sequence G1-G2-G3 (Gas 1, Gas 2, and Gas 3) refers to the impregnate gas filter position in the holder.

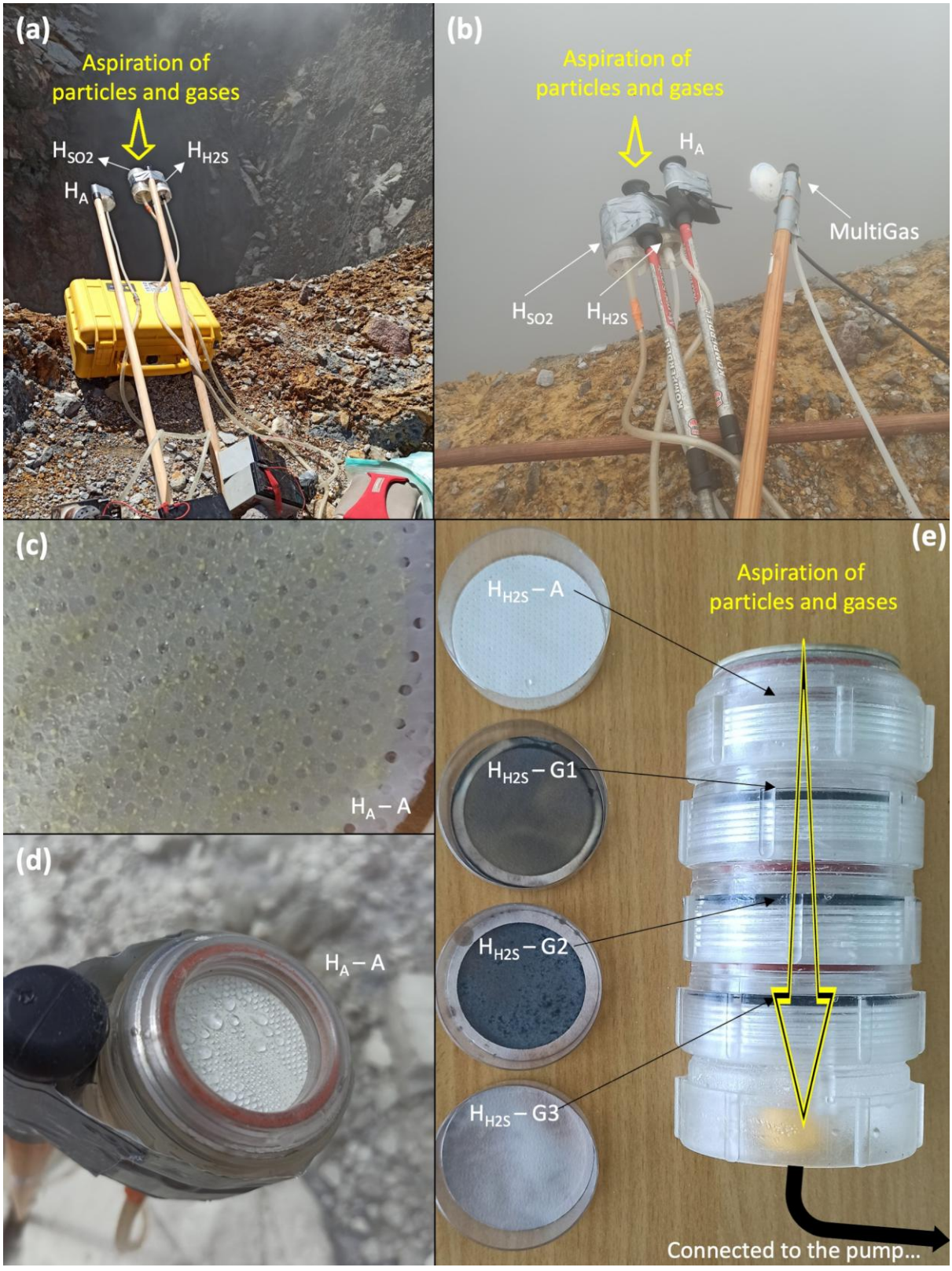

186

187 **Figure 3** Filter pack assemblage for plume sampling procedures at La Soufrière volcano: a) Sampling
188 during less humid (RH 80 %, August 25, 2021) weather conditions, b) Sampling during humid (RH 92%,
189 July 19, 2021) conditions, c) View of a PTFE filter exposed 60 min in less humid conditions, d) View of a

PTFE filter exposed 60 min in humid conditions, and e) General view of the H_{H2S} after 15 min plume exposure: dark brownish filters denote the reaction of H_2S with $AgNO_3$ from gas filters.

The treatment of gas filters was carried out in the chemistry laboratory of the Observatoire Volcanologique et Sismologique de la Guadeloupe of the Institut de Physique du Globe de Paris (OVSG-IPGP), while analyses for major anions were carried out at the IPGP in Paris. Before analyses, $NaHCO_3$-treated filters were eluted with 20 ml of Milli-Q water and left at ambient temperatures for one week. Subsequently, the sample was analyzed by ionic chromatography (Dionex Integrion™) to determine the concentration of sulfate. These filters were not oxidized because $NaHCO_3$ can react with H_2S producing HS^- in the presence of condensed steam or very humid conditions (Garner et al. 1958; Deng et al. 2019); oxidation of $NaHCO_3$-treated filters would in turn overestimate sulfate concentrations. $AgNO_3$-treated filters were put into Teflon beakers and eluted twice with a mixture of diluted HNO_3 (19 ml, 2 vol.%) plus H_2O_2 (1 ml, 60 vol.%) on a hot plate (~80 °C) until dry. Subsequently, the residue was eluted with 20 ml of Milli-Q to determine the concentration of H_2S as sulfate via ionic chromatography. Internal calibrations determined an analytical error of <5%.

PTFE filters were treated for analysis in a chemistry clean room hosted in the Laboratoire de Magma et Volcans (Université Clermont Auvergne, France). First, they were hot-leached in clean Teflon beakers using 5 ml of a solution containing HF (0.05 M) and HNO_3 (0.4 M). Then, extracts were transported to the IPGP to be analyzed for trace elements through an Inductively Coupled Plasma Quadrupole Mass Spectrometer (ICP-QMS, Agilent 9000). Internal standards (Sc, In, and Re) were used to control instrument deviation. The analytical error was <10%.

Non-treated PTFE filters were cut into ~8 × 8 mm squares, mounted on carbon tape-covered aluminum holders, coated with carbon, and analyzed using Scanning Electron Microscope with Energy Dispersive Spectrometer (SEM-EDS, Quanta 250) in the C3-Mag laboratory at the Université des Antilles (Pointe-à-Pitre, Guadeloupe). Following this, highest resolution images were retrieved using a Field Emission Gun (FEG) – SEM (Auriga 40, Zeiss) at the IPGP. Semi-quantitative chemical analyses were performed in the EDS mode using 15 kV of acceleration voltage, 3-5 nA beam current, 40 s dwell time, and 8.5-10 mm working distance. The acquisition of high-resolution imaging and data processing was made using INCAEnergy and Spirit2 software.

Table 1 Summary of measurements carried out at La Soufrière volcano; the sampling site, holder type, pump flow rate (l/min), filtered volume (m^3), and distance from the vent have been listed.

Date	Fumarole	Set up	Holder type	Pump flow rate (l/min)	Volume (m^3)	Distance from the vent (m)	Relative Humidity (%)
29/01/2021	CS	A+G1+G2*$^{\$}$	H_{SO2}	6.7	0.134	5	84
		A+G1+G2$^{\$}$	H_{H2S}	12	0.18		

29/01/2021	NapN	A+G1+G2*[$] A+G1+G2[$]	H_{SO2} H_{H2S}	6.7 12	0.134 0.18	3	88
12/02/2021	CIT	A+G1+G2	-	12	0.84	1400**	84
16/03/2021	CS	A+G1+G2+G3 A+G1+G2+G3 A*	H_{SO2} H_{H2S} H_A	6.7 7 12	0.1139 0.119 -	5	90
04/06/2021	CS	A G1+G2+G3 A+G1+G2+G3 P	H_{SO2} H_{H2S} H_A	7 6.7 12	0.175 0.1005 0.6	5	95
15/06/2021	CS	A+G1+G2+G3 A+G1+G2+G3* A	H_{SO2} H_{H2S} H_A	7 6.7 12	0.175 0.1005 0.72	5	85
15/06/2021	NapN	A+G1+G2+G3* A+G1+G2+G3 A	H_{SO2} H_{H2S} H_A	6.7 7 12	0.1675 0.105 0.54	3	85
19/07/2021	CS	A+G1+G2+G3 A+G1+G2+G3* A*	H_{SO2} H_{H2S} H_A	7 6.7 12	0.196 0.1139 -	5	91
19/07/2021	G56	A+G1+G2+G3* A+G1+G2+G3 A	H_{SO2} H_{H2S} H_A	7 6.7 12	0.175 0.1072 0.744	10	92
25/08/2021	CS	A+G1+G2+G3* A+G1+G2+G3 A	H_{SO2} H_{H2S} H_A	7 6.7 12	0.175 0.1005 0.72	5	80
25/08/2021	G56	A+G1+G2+G3 A+G1+G2+G3* A	H_{SO2} H_{H2S} H_A	6.7 7 12	0.1675 0.105 0.72	10	80
22/09/2021	CS	A+G1+G2+G3 A+G1+G2+G3* A	H_{SO2} H_{H2S} H_A	6.7 7 12	0.1675 0.105 0.72	5	49
22/09/2021	G56	A+G1+G2 A+G1+G2+G3* A	H_{SO2} H_{H2S} H_A	6.7 7 12	0.1675 0.105 0.72	10	63

*Particle filters used only for SEM observations; **Distance from the volcano summit; [$]Gas filters were only used for sampling tests to constrain humidity effects, sampling time, and filter saturation. The relative humidity (RH) during sampling was taken from the "Sanner" weather station, which is located at the volcano summit.

3.2 MultiGas

Fluxes of major gas compounds emitted from degassing volcanoes are usually measured by ground-based remote techniques such as Differential Optical Absorption Spectroscopy (DOAS) or UV cameras. These techniques allow reliable fluxes of SO_2 to be obtained. However, these techniques cannot be applied to La Soufrière de Guadeloupe, where fumarolic emissions contain negligible amounts of SO_2 but high concentrations of H_2S. Consequently, we used a MultiGas device (Aiuppa et al. 2005a; Shinohara 2005) to measure H_2S fluxes in the volcanic plume following the method proposed by Allard et al. (2014) and Tamburello et al. (2019).

MultiGas is a portable multi-sensor system that allows fast measurement of primary gas compounds in volcanic plumes. This device included a Gascard IR spectrometer for CO_2 determination (calibration range: 0–3000 ppmv; accuracy: ± 2%; resolution: 0.8 ppmv) and City Technology electrochemical sensors for SO_2 (sensor type 3ST/F; calibration range: 0–200 ppm, accuracy: ± 2%, resolution: 0.1 ppmv) and H_2S

(sensor type 2E; range: 0–200 ppm, accuracy: ±5%, resolution: 0.7 ppmv). It has a GPS attached that enables the device's position to be tracked at 1 Hz refresh rate. To determine fumarolic gas fluxes from the two main vents where the fumarolic emissions were strong enough to generate a plume (CS and G56), the horizontal and vertical distributions of gas species in the plume cross-sections were measured at two different heights (typically 0.9 and 2 m) during walking traverses orthogonal to the plume direction, a few meters downwind from the vents. Observations suggest that the fumarolic emissions were mostly flattened to the ground by strong trade winds (up to 14 m/s), and their upper boundary stood at ca. 3-4 m above the ground with a maximum gas density centered at 1.5-2 m above the ground (Gaudin et al. 2016; Tamburello et al. 2019). Wind speed was measured with a portable anemometer at the same height as the MultiGas inlet during all traverses. These measurements were carried out contemporaneously with the filter pack sampling.

CO_2/H_2S and SO_2/H_2S gas ratios were processed with the least squared method using the RatioCalc software (Tamburello 2015). We interpolated the concentration measurements for CS and G56 using a 2D spline function and then integrated them over the plume cross section to obtain Integrated Concentration Amounts (ICAs) using RatioCalc software (Tamburello 2015). These computations were based on CO_2 as a volcanic marker (ICA CO2; Table 4), given that the IR CO_2 sensor reacts faster than the H_2S sensor and CO_2 measurements are not affected by high humidity conditions (Tamburello et al. 2019). Subsequently, CO_2 fluxes were computed by scaling the obtained CO_2 concentration in plume cross sections with the average wind speed. Finally, H_2S was computed by scaling the average H_2S/CO_2 weight ratio with the CO_2 flux (Moune et al. 2022). These flux computations carry an approximate error of 40% (Tamburello et al. 2014), attributed by uncertainties in the average wind speed measurements.

4 RESULTS

4.1 Physicochemical characterization of solid particles

The type, morphology, and chemistry/mineralogy of particles transported within the plume at La Soufrière volcano were investigated. The appearance of PTFE filters during and after the sampling featured significant amounts of small yellowish particles (Fig. 3c), a few dark particles, and droplets (Fig. 3d). No evident correlation between sampling time and the number of particles was noted. Longer exposures however have the ability to potentially enhance the possible leaching of the filters, resulting in microscopic observations evidencing a circular distribution of solid particles (Fig. 4), a couple of weeks after sampling. Such distribution suggests that droplets gently evaporated during storage.

The size of the solid particles on filters was measured to be up to 310 µm, and found as subrounded droplet marks or scattered on the filter (Fig. 4; Supplementary Material 1). In general, solid particles appeared abundantly in CS filters than in NapN or G56 filtes, likely due to the stronger degassing and hence more erosive contribution at CS. Based on the physicochemical characteristics of particles (Supplementary Material 1), they can be divided into three groups: i) Sulfur-bearing particles that measured up to 310 µm in size and were commonly found in CS samples, corresponding to native sulfur and sulfates interpreted as

thenardite (Na_2SO_4) and gypsum ($CaSO_4 \cdot 2H_2O$; Fig. 5). In the case of gypsum, the presence of bassanite ($CaSO_4 \cdot 0.5H_2O$) and anhydrite ($CaSO_4$) cannot be fully discarded; ii) Cl-bearing fragments that reached up to 230 µm in size (were more common in NapN filters), composed of halite (NaCl), sylvite (KCl), and possible akaganeite ($Fe^{3+}O(OH,Cl)$; Fig. 5), in addition to several unidentified Cl-bearing particles together with Mg, Na, S, and K, suggesting the possible formation of chlorosulfate complexes or small phases with variable chemical composition (Supplementary Material 1); and iii) rock particles (up to 200 µm) rich in Si and other lithophile and siderophile chemical elements (Mg, Ca, K, Ti, Mn, and Fe), which appeared in similar proportions as in CS and NapN filters, but predominated in G56 samples.

It is also important to note that some unusual Fe-bearing particles were found on the filters. For example, a Fe-O (48 and 47 wt.%, respectively) particle with traces of Mn, S, Cl, and K was found on NapN filters, which could be linked with hematite (Fe_2O_3), although EDS analyses were inconclusive. Similarly, <10 µm Fe-Cr (88.3 and 11.7 wt.%, respectively) particles were also found on CS filters, which could correspond to chromferide ($Fe_3Cr_{0.4}$) or iron-rich particles of unknown origin; their possible anthropogenic origin could be discarded since there is no presence of steelworks or port activities that potentially contribute solid particles at the volcano summit. In addition, other heavy metals such as, Cu, Zn, and Sb, occasionally appeared in low concentrations (<15 wt.%; Fig. 5d, e) in one CS and one NapN sample.

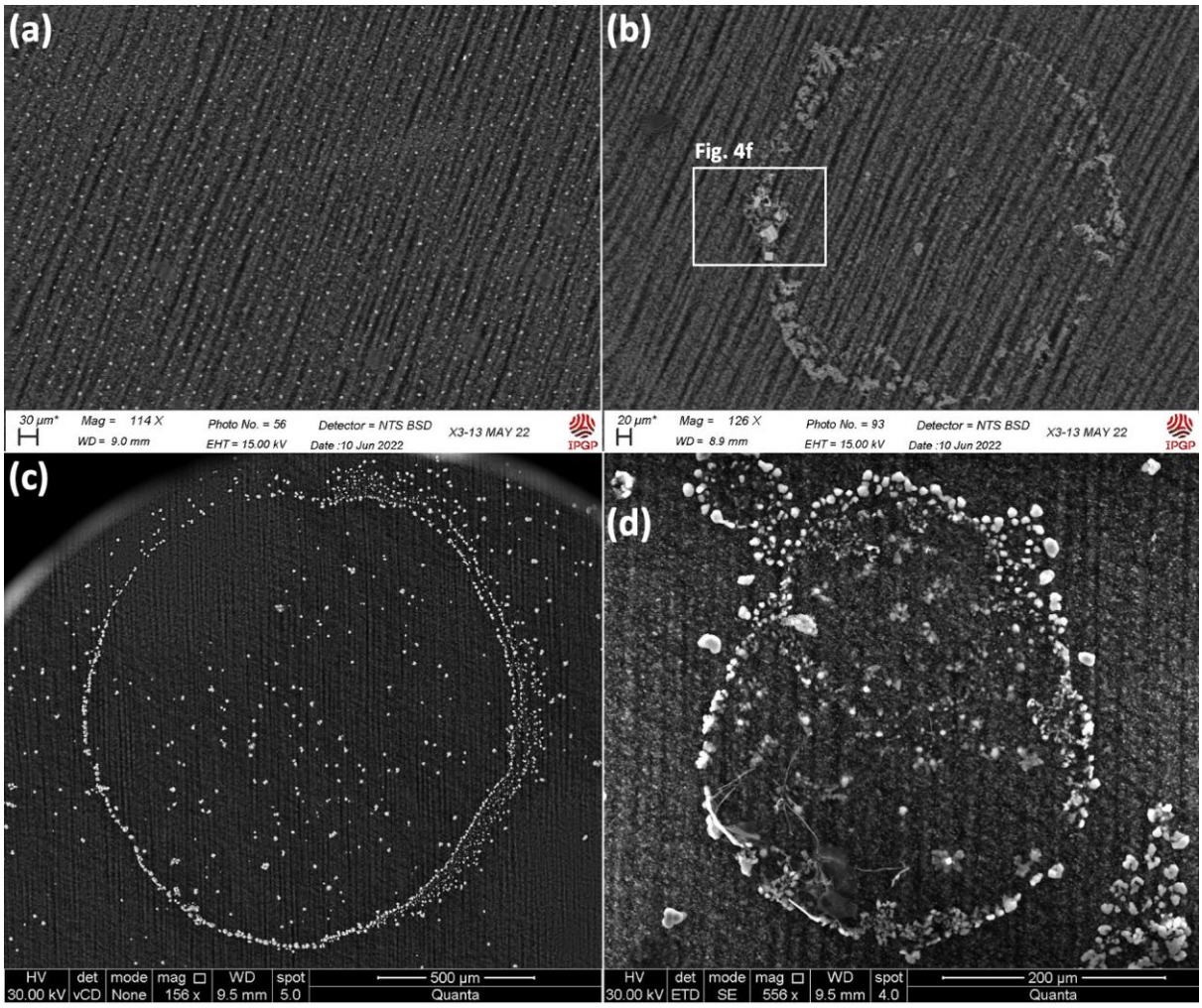

Figure 4 General view of PTFE aerosol filters. a) filter non-affected by humidity, while b), c), and d) correspond to filters collected during more foggy and humid conditions. The filter dryness caused rounded droplet marks with the distribution of solid particles.

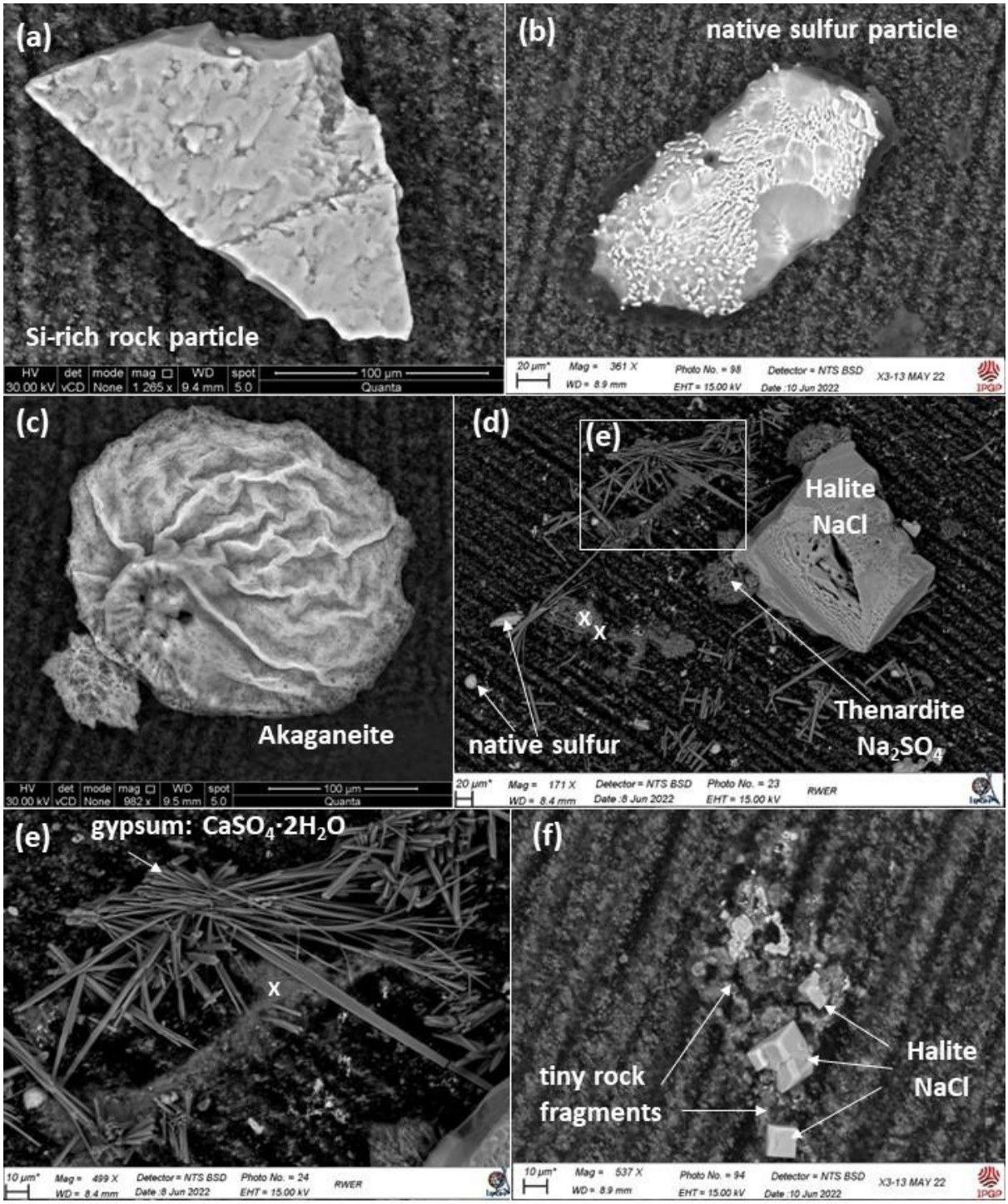

Figure 5 Morphology (SEM-BSE) and chemistry of representative solid particles on aerosol filters. Images with "x" marks represent point analyses with noticeable concentrations of Zn. Point EDS analyses are presented in Supplementary Material 1.

296 4.2 Major and trace element concentrations

297 Major and trace element concentrations in filter pack holders H_A and H_{H2S} from CS, G56, and NapN
298 plumes and average relative humidity during sampling have been presented in Table 2 and Supplementary
299 Material 2. H_{SO2} holders were not considered because they showed more enhanced Na, Cl, Ca, and Mg
300 concentrations which are likely more related to impurities in our alkaline solution ($NaHCO_3$) instead of a
301 volcanic source. As expected, and considering their longer sampling duration, H_A aerosol filters displayed
302 higher average concentrations than H_{H2S} aerosol filters, suggesting negligible leaching effects as exposure
303 time increased. Nevertheless, possible leaching effects due to humid climatic conditions at the volcano
304 summit, besides the high concentration of steam in fumarolic emissions, cannot be ruled out. Thus major
305 and trace element concentrations presented in this work must be considered as minimum values.

306 The reliability of the data can be evaluated based on the relative standard deviation (RSD) percentage. This
307 expression is a comparison between the standard deviation and the mean of the sample. An RSD >33%
308 (value equal to three standard deviations) suggests the presence of concentrations below the detection
309 limit. Consequently, samples with higher RSD should be discarded due to their lower reliability. Chemical
310 analyses from this study reported very low RSD values for various chemical elements. For example, B, Na,
311 Mg, Al, Si, Cl, Ca, Ti, V, Cr, Mn, Fe, Co, Cu, Zn, Rb, Sr, Y Zr, Sn, Sb, Ba, La, Ce, Pr, and Pb presented
312 average RSD <5%, while Li, K, Ni, As, Mo, Cs, Nd, Eu, Tb, Ho, Hf, Tl, Th, and U reported average RSD
313 of 5-10%. S, Ga, Se, Br, Nb, Cd, Te, Sm, Gd, Dy, Er, Tm, Yb, Lu, Ta, W, and Bi presented 10-33% RSD.
314 Moreover, Be, P, Ge, I, and Hg reported higher RSD (>33%), ascribed to concentrations close to or below
315 the detection limit or analytical difficulties (Jian et al. 2000; Badocco et al. 2017). Hence, chemical
316 elements with RSD >33% were removed to attain a representative and confident dataset, and their
317 concentrations were converted into "below detection limit" ("bdl"; Table 2).

318 Data were processed following chemical and atmospheric background corrections (Supplementary
319 Material 2). The chemical blank accounted for 5-10% of average major and trace element concentrations,
320 except for Mo (16%), Sr (20%), Ca (27%), Cr (70%), and Ba (235%). At the same time, the atmospheric
321 background (atmospheric blank in Supplementary Material 2) contained concentrations less than 10% of
322 the average major and trace element concentrations, except for U (12%), Li (13%), Ni (13%), Tb (15%),
323 Mn (17%), Cu (20%), Bi (20%), Ta (23%), Co (24%), Mg (28%), V (28%), Rb (28%), Cr (36%), Tl
324 (37%), W (45%), K (51%), and Mo (58%). The average chemical concentrations of Cl and Pb were found
325 to be similar in the atmospheric blank and volcanic plumes. Na and Cd concentrations were removed from
326 Table 2 because marine aerosols strongly influence Na, and Cd presented higher concentrations in the
327 atmospheric blank than in aerosol filters (0.84 versus an average of 0.17 ng/m^3 of Cd; Supplementary
328 Material 2). These enhanced concentrations suggested that the Guadeloupean atmosphere could be
329 enriched in Li, Mg, Na, K, V, Cr, Fe, Cu, Cl, Rb, Mo, Cd, Tb, Ta, W, Tl, Bi, and Pb; careful attention
330 should thus be given to this non-volcanic source of trace elements in fumarolic plumes. Accordingly, blank
331 atmospheric concentrations were subtracted from the total concentrations measured in aerosol filters to
332 obtain plume-specific concentrations (Supplementary Material 2).

Considering both chemical and atmospheric blanks, the corrected concentration of major and trace elements in the fumarolic plumes at La Soufrière ranged from 10^6 to 10^{-2} ng/m^3 (Table 2). Chlorine reached the highest concentrations (10^6 ng/m^3), followed by concentrations of 10^4 ng/m^3 for Si, S, and Fe. Then, B, Mg, Al, K, Ca, Ti, Cr, Zn, and Br reached plume concentrations of 10^2-10^4 ng/m^3. Vanadium, Mn, Ni, Cu, As, Sr, Zr, Mo, Sn, Sb, I, and Pb had in concentrations of ~10^1 ng/m^3, while Li, Co, Ga, Ge, Rb, Y, Nb, REEs, Hf, Ta, Tl, Bi, Th, and U were <1 ng/m^3. Compared to G56, fumarolic plumes from NapN and CS displayed slight enrichments in the average chemical concentrations compared with G56, likely due to the shorter sampling distance from the vent. Despite the high concentrations of Cl, data curation allowed its purely volcanic recognition only in two (one sample in CS and another from G56) of the eleven samples (Table 2). Ag was only detected in H_{H2S} (Supplementary Material 2), which indicates possible contamination from $AgNO_3$-gas filters; Ag was thus removed from the representative dataset (Table 2).

Table 2 Corrected chemical concentration of major and trace elements (expressed in ng/m^3) from aerosol filters after RSD treatment, chemical, and atmospheric background corrections (Supplementary Material 2).

Site	**CS**	**CS**	**CS**	**CS**	**CS**	**CS**	**G56**	**G56**	**G56**	**NAPN**	**NAPN**
RH	**84**	**90**	**95**	**85**	**80**	**49**	**92**	**80**	**63**	**84**	**85**
Filter	**H_{H2S}**	**H_{H2S}**	**H_A**	**H_A**	**H_A**	**H_A**	**H_A**	**H_A**	**H_A**	**H_{H2S}**	**H_A**
Date	**29/01/ 2021**	**16/03/ 2021**	**04/06/ 2021**	**15/06/ 2021**	**25/08/ 2021**	**22/09/ 2021**	**19/07/ 2021**	**25/08/ 2021**	**22/09/ 2021**	**29/01/ 2021**	**15/06/ 2021**
Li	0.27	bdl	2.07	1.20	1.10	0.19	0.28	0.40	0.13	0.72	1.35
Be	bdl	bdl	bdl	0.08	bdl	bdl	bdl	bdl	0.02	bdl	bdl
B	bdl	bdl	bdl	52	90	2339	1.26	bdl	6.58	bdl	bdl
Mg	232	153	130	301	828	35	169	302	64	540	361
Al	671	194	565	3874	2989	1331	745	1413	582	1070	3048
Si	2050	203	3383	19257	14520	4642	2439	5142	3104	2458	7421
S	bdl	24254	2657	bdl	5512	4060	2747	1423	12515	9148	bdl
Cl	bdl	840348	bdl	bdl	bdl	bdl	bdl	bdl	87169	bdl	bdl
K	242	bdl	388	307	385	bdl	bdl	67	bdl	856	423
Ca	1036	bdl	4660	48	876	556	883	2403	bdl	6974	1352
Ti	79	42	28	281	204	141	19	1073	70	65	98
V	2.08	3.20	1.23	9.38	7.68	2.34	6.67	12	0.75	2.92	9.19
Cr	411	478	74	8.51	bdl	bdl	bdl	bdl	bdl	262	bdl
Mn	6.82	6.66	14	16	44	8.86	19	27	5.34	15	29
Fe	348	15	1500	5834	6174	3168	10367	13265	1377	1248	10256
Co	0.06	0.79	0.45	0.77	0.86	0.16	0.45	1.03	0.06	0.24	0.89
Ni	2.58	29	48	1.72	5.98	bdl	2.59	1.64	bdl	9.99	13
Cu	1.30	1.67	115	8.26	42	bdl	8.11	bdl	bdl	85	35
Zn	239	122	1352	20	600	2	60	37	78	938	537
Ga	bdl	bdl	0.29	1.08	0.84	0.51	bdl	0.55	0.21	0.37	1.01
Ge	bdl	bdl	bdl	0.18	0.24	bdl	bdl	bdl	bdl	bdl	bdl
As	7.46	bdl	1.78	0.62	1.44	0.27	0.45	0.50	0.17	21	1.31
Se	bdl	3.04	0.39	bdl	1.55	0.84	2.14	0.89	2.64	1.94	1.10
Br	bdl	bdl	bdl	477	559	4459	321	bdl	bdl	bdl	bdl
Rb	0.30	0.21	0.47	2.25	1.88	0.12	0.04	0.68	0.16	0.91	1.87
Sr	6.45	bdl	4.58	3.12	5.89	4.28	1.38	5.40	1.17	15	5.90
Y	0.21	0.12	0.20	0.50	0.79	0.14	0.23	0.46	0.16	0.29	0.62
Zr	6.76	1.74	13	7.15	4.12	0.69	0.40	2.39	0.78	1.88	2.69
Nb	bdl	bdl	0.09	0.62	0.52	0.11	bdl	0.88	0.10	bdl	0.84
Mo	bdl	5.20	0.28	bdl	0.50	bdl	bdl	3.85	bdl	bdl	1.25
Sn	1.15	0.03	26	1.22	35	1.03	12	0.69	0.58	7.04	28
Sb	0.71	179	9.98	158	10	3.61	0.17	0.15	0.30	3.02	5.19
Te	0.35	bdl	0.02	0.11	0.08	bdl	bdl	0.03	bdl	0.70	bdl
Cs	0.44	bdl	0.03	0.16	0.11	0.02	0.02	0.05	0.02	0.75	0.13
Ba	bdl	bdl	bdl	bdl	2.59	bdl	bdl	bdl	bdl	bdl	bdl
La	0.324	0.208	0.265	1.030	0.965	0.209	0.247	0.802	0.233	0.500	1.022
Ce	0.636	0.442	0.437	2.006	1.878	0.454	0.595	1.618	0.493	0.901	2.346

Pr	0.060	0.044	0.037	0.221	0.186	0.047	0.049	0.178	0.050	0.089	0.239
Nd	0.255	0.204	0.184	0.845	0.808	0.199	0.234	0.767	0.204	0.347	0.975
Sm	0.064	0.071	0.072	0.156	0.167	0.047	0.059	0.167	0.042	0.099	0.207
Eu	bdl	bdl	0.009	0.033	0.036	0.014	0.011	0.030	0.010	0.021	0.042
Gd	bdl	bdl	0.044	0.125	0.157	0.043	0.058	0.134	0.038	0.206	0.162
Tb	0.006	0.005	0.006	0.019	0.022	0.004	0.006	0.017	0.005	0.011	0.021
Dy	0.039	0.026	0.036	0.105	0.144	0.025	0.047	0.105	0.032	0.055	0.124
Ho	bdl	bdl	0.007	0.021	0.029	0.005	0.008	0.017	0.006	0.011	0.023
Er	0.032	bdl	0.026	0.066	0.102	0.021	0.034	0.055	0.023	0.045	0.069
Tm	0.004	bdl	0.003	0.010	0.014	0.002	0.004	0.008	bdl	0.007	0.010
Yb	0.021	0.010	0.022	0.062	0.089	0.016	0.028	0.062	0.018	0.025	0.061
Lu	bdl	bdl	0.004	0.009	0.015	0.002	0.004	0.009	0.003	0.004	0.009
Hf	0.17	0.07	0.28	0.19	0.11	0.02	0.01	0.08	0.02	0.07	0.08
Ta	bdl	bdl	0.04	0.04	0.01	bdl	bdl	0.14	bdl	0.12	0.11
W	0.22	1.06	0.35	bdl	0.14	bdl	bdl	0.22	bdl	0.87	0.21
Tl	0.10	0.23	0.00	0.01	0.02	bdl	0.00	bdl	0.02	0.20	0.01
Pb	bdl	0.66	4.97	bdl	2.78	bdl	bdl	bdl	bdl	3.94	0.85
Bi	1.09	bdl	0.18	bdl	0.01	bdl	bdl	bdl	bdl	1.98	0.09
Th	bdl	0.06	0.05	0.29	0.24	0.07	0.07	0.42	0.07	0.10	0.28
U	0.01	0.01	0.01	0.06	0.05	0.02	0.03	0.05	0.01	0.04	0.06

bdl: below detection limit

4.3 Major gas ratios and H_2S volatile fluxes

Gas ratios were measured using filter pack and MultiGas techniques. Plumes were reportedly flat during the sampling period because of persistent west-northwestern wind blowing at 4.2 m/s on average (maximum of 9.5 m/s), while windless days prompted vertical plumes generating unreliable data. Similarly, the high relative humidity may have been responsible for production of partial leaching on the G1 filter (Figs. 2 and 3), as seen at the end of the sampling on the wettest days.

Theoretically, chemical concentration should decrease from G1 to G3 (Fig. 3e and Table 1), with G1 containing approximately 90% of the total sulfate concentration (Pennisi and Le Cloarec 1998), whereas G2 and G3 having negligible concentrations (<10%). The non-negligible concentration in the last gas filter indicates filter saturation, which does not represent a valid measurement (Wittmer et al. 2014). At La Soufrière, intervals of total sulfate concentrations (i.e., G1+G2+G3 concentrations) in H_{SO2} and H_{H2S} gas filters were 25.7-1486 and 457-4692 ppm (Table 3), respectively, with concentrations generally decreasing from G1 to G3 (Fig. 6). However, six gas samples (four from H_{SO2} and two from H_{H2S}, Fig. 6) displayed saturation because the G3 filter contained sulfate concentrations >10%, and hence, were discarded. In contrast, for the non-saturated samples ($G3_{H2S}$, $G3_{SO2}$ <10%), G1-H_{SO2} accumulated between 77 and 91% of the total sulfate concentration, while G1- and G2-H_{H2S} retained more similar sulfate concentrations (56 and 41%, respectively), with G2-H_{H2S} occasionally presenting higher concentrations than G1-H_{H2S}. These equivalent concentrations potentially suggest that the trapping efficiency of G1-H_{H2S} decreased with humidity, while that of $NaHCO_3$-gas filters remained less affected. We thus reccomend the adoption of three gas filters for sampling tropical wet volcanic plumes based on significant concentrations found in G2-H_{H2S} filters.

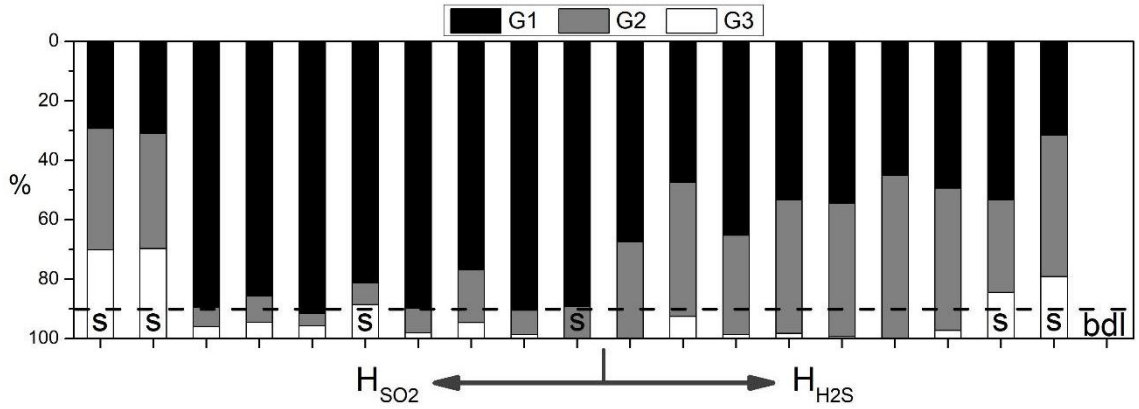

Figure 6 Sulfate concentration (%) in each gas filter (G1, G2, and G3) with respect to the total amount of sulfate in H_{SO2} and H_{H2S}. The horizontal black dashed line at 90% bounds saturated ("s") filters: when G3 occupies more than 10% of the total concentration of sulfate. Percentages for the G56 sample collected in September 2021 (H_{H2S}) presented concentrations below the detection limit (bdl).

Ratios involving sulfur help constrain magmatic and hydrothermal contributions to gas emissions at quiescent degassing volcanoes. Here we measured SO_2/H_2S molar ratios in air-diluted samples from the CS, NapN, and G56 sites using filter packs and MultiGas techniques (Tables 3 and 4, Supplementary Material 3). In the case of CS, SO_2/H_2S ratios determined by filter packs and MultiGas were within the range of 0.18-0.94 and 0.066-0.19, respectively (Table 3), at NapN, they were 0.61 (Table 3) and 0.06 (Séverine Moune, personal communication), respectively. Finally, G56 MultiGas ratios ranged from 0.018 to 0.039, while simultaneous filter pack measurements were saturated (Table 3). A comparison of filter packs and MultiGas SO_2/H_2S showed evidenced that the results obtained using the filter pack technique were up to one order of magnitude higher than those reported by MultiGas. Such higher SO_2/H_2S ratios in filter packs are not representative of gas, especially considering the low and stable SO_2 concentrations and fluxes over the years (Table 4; Moune et al. 2022). Discrepancies can be mainly attributed to sampling issues such as, i) partial oxidation of sulfur species during sample preparation prior to ionic chromatography analyses or ii) enhanced trapping of S-compounds favored by the wetness of gas filters (Mioduszewski and Kress 2008) of the filter pack technique.

H_2S fluxes measured during discrete field campaigns in 2021 were found to be within the 0.67-2.83 t/d range at CS and 0.27-0.74 t/d at G56. These values have remained stable since mid-2018 after higher fluxes occasionally measured in 2016-2017 (Tamburello et al. 2019). Dry gas fluxes reported in CS were twice higher than those of G56 (Supplementary Material 3).

Table 3 Total sulfate concentration and molar ratios obtained from filter packs in CS, NapN, and G56 plumes (Supplementary Material 3). Holders in which the third gas filter contained more than 10% of the total sulfate concentration are namely "saturated". Total sulfate concentrations are normalized values considering 1 m^3 of volcanic plume.

Site	Date	FP	Total sulfate ppm	SO_2/H_2S molar ratio
CSC	16/03/2021	$P(SO_2)$	saturated	N/A
		$P(H_2S)$	457.15	
CSC	04/06/2021	$P(SO_2)$	saturated	N/A
		$P(H_2S)$	4692.88	
CSC	15/06/2021	$P(SO_2)$	1240.07	0.743
		$P(H_2S)$	3136.53	
NapN	15/06/2021	$P(SO_2)$	266.95	0.610
		$P(H_2S)$	823.09	
CSC	19/07/2021	$P(SO_2)$	213.83	0.184
		$P(H_2S)$	2179.20	
G56	19/07/2021	$P(SO_2)$	Saturated	N/A
		$P(H_2S)$	1634.49	
CSC	25/08/2021	$P(SO_2)$	1486.12	0.942
		$P(H_2S)$	2967.09	
G56	25/08/2021	$P(SO_2)$	36.65	N/A
		$P(H_2S)$	saturated	
CSC	22/09/2021	$P(SO_2)$	684.56	N/A
		$P(H_2S)$	saturated	
G56	22/09/2021	$P(SO_2)$	saturated	N/A
		$P(H_2S)$	bdl	

bld: below detection limit; N/A: not applicable.

Table 4 Average wind speed, average SO_2/H_2S molar ratios, and H_2S fluxes emitted from CS and G56 vents. H_2S fluxes were obtained using the Integrated Concentration Amounts (ICA) for CO_2 (ICA CO2), the latter being considered as the volcanic marker (Section 3.2). Dry gas fluxes were obtained by adding the three main fluxes (but not water flux; Supplementary Material 3).

Date	Wind speed*	Molar ratios		H_2S max	ICA CO2	Flux (t/d)			
	m/s	SO_2/H_2S	CO_2/H_2S	ppm	(ppm/m^2)	CO_2	H_2S	SO_2	Dry gas
Cratere Sud									
*2006 & 2012	-	0.035	2.50	-	-	-	-	-	-
*2016-2017	-	0.003	3.32	106	7143	5.23	1.87	0.01	7.10
*2018-2020	-	0.067	2.78	75	6923	3.86	1.04	0.05	4.93
16/01/2021	3.8	-	3.300	167	8134	4.81	1.13	-	5.93
29/01/2021	2.35	0.066	2.700	130	6430	2.35	0.67	0.08	3.11
16/03/2021	3.06	0.163	3.060	188	12500	5.95	1.50	-	7.45
04/05/2021	3.48	-	2.005	85	7584	4.10	1.58	0.49	6.17
04/06/2021	4.36	0.166	2.341	116	12662	8.59	2.83	-	11.42
19/07/2021	3.3	0.191	1.855	64	5336	2.74	1.14	0.41	4.29
22/09/2021	2.8	0.162	1.821	111	10861	4.73	2.01	0.61	7.35

27/10/2021	3.2	0.080	1.993	198	11376	5.66	2.20	0.33	8.19
Gouffre 56									
*2006 & 2012	-	-	-	-	-	-	-	-	-
*2016-2017	-	0.012	3.78	33	4165	4.53	1.27	0.02	5.81
*2018-2020	-	0.036	3.49	22	2766	2.01	0.48	0.03	2.52
16/01/2021	8.1	-	5.120	7	2484	3.13	0.47	-	3.60
29/01/2021	2.6	0.062	3.480	27	3040	1.23	0.27	0.03	1.53
16/03/2021	4.52	0.034	3.420	22	4652	3.27	0.74	0.08	4.09
04/05/2021	7.6	-	4.113	17	2004	2.37	0.44	0.03	2.84
04/06/2021	9.47	0.039	3.919	9	2125	3.13	0.62	0.05	3.79
19/07/2021	5.8	0.036	3.898	7	1906	1.72	0.34	0.02	2.08
22/09/2021	2.8	0.030	3.305	29	5417	2.36	0.55	0.03	2.94
27/10/2021	3.9	0.018	3.324	22	4354	2.64	0.61	0.02	3.28
TOTAL (Cratere Sud + Gouffre 56)									
16/01/2021	-	-	-	-	10618	7.94	1.60	0.00	9.53
29/01/2021	-	-	-	-	9470	3.58	0.95	0.12	4.64
16/03/2021	-	-	-	-	17152	9.22	2.24	0.08	11.54
04/05/2021	-	-	-	-	9588	6.47	2.03	0.51	9.01
04/06/2021	-	-	-	-	14787	11.72	3.45	0.05	15.21
19/07/2021	-	-	-	-	7242	4.46	1.48	0.43	6.37
22/09/2021	-	-	-	-	16278	7.09	2.56	0.64	10.29
27/10/2021	-	-	-	-	15730	8.30	2.81	0.35	11.46

* represent average ratios and fluxes previously published from CS and G56 sites (Allard et al. 2014; Tamburello et al. 2019; Moune et al. 2022).

5 DISCUSSIONS

5.1 Origin of airborne solid particles

The S-, Cl-, and Si-bearing particles on top of La Soufrière appear to be primarily volcanic in origin mainly because these particles were trapped a few meters from fumarolic vents that were already characterized for emitting these particles (Inostroza et al. 2022a, b). However, additional particle sources related to Saharan, marine, or anthropogenic contributions cannot be entirely discarded. The atmospheric background measurement (sample "CIT", Table 1) shows significant concentrations of trace elements, despite the absence of solid volcanic particles on the aerosol filter. Furthermore, the Guadeloupe archipelago have been know to get polluted by sea salt aerosols rich in Na, Cl, K, Mg, S, and Ca (Dessert et al. 2015; Xu-Yang et al. 2022) and affected by Saharan dust every year, especially between April and September (Muhs et al. 1990; Pett-Ridge 2009; Dessert et al. 2020; Xu-Yang et al. 2022), transporting solid microparticles through the Atlantic Ocean and enriching the Guadeloupean environment in Si, Al, Ca, K, and Fe.

The transport and concentration of non-volcanic aerosols in island environments are mainly governed by wind speed, relative humidity, rainfall regime, altitude above sea level, and particle diameter (Shinozuka et

al. 2004; Prather et al. 2013; Murphy et al. 2019). The latter becomes preponderant discriminating non-S-rich aerosols found in the volcanic plume at La Soufrière (Dusek et al. 2006). For example, a significant number of solid particles found in the plume (Figs. 5 and 6) display predominantly larger diameter above 10 µm and up to 300 µm in comparison with worldwide marine aerosols that generally are <3 µm (Chabas and Lefèvre 2000; O'Dowd and de Leeuw 2007) or Saharan particles usually <10 µm (Petit 2005; Euphrasie-Clotilde et al. 2021), suggesting a predominant volcanic origin of the largest particles. However, it is believed that <10 µm aerosols (called PM10) of non-volcanic origin (mainly marine) rich in Na, Cl, K, Mg, S, and Ca could impact the concentration of these elements in the volcanic plume of La Soufrière, substantiating the need for study atmospheric blanks. Moreover, pollution peak events related to Saharan dust provoked PM_{10} concentrations >50 $\mu g/m^3$ (www.gwadair.fr). Particularly, the event on June 15 and July 19, 2021 (www.gwadair.fr) could have influenced the sampled plume's composition. However, such events did not cause noticeable increases in Al, Ca, K, or Fe concentration as could have been expected. Undoubtedly, more detailed information is needed to constrain their contributions and effects during plume sampling.

Sulfates and Cl-bearing minerals are usually deposited directly from the gas phase in high temperature (above 400 °C) magmatic emissions (e.g., Getahun et al. 1996; Africano et al. 2002; Nekvasil et al. 2019). However, their presence in low-temperature hydrothermal emissions implies multiple processes, such as gas phase condensation, leaching of host rocks, and precipitation of S-bearing species under more oxidizing conditions (Africano and Bernard, 2000; Zimbelman et al., 2005). Halides can be formed by gas phase condensation followed by cooling or evaporation of magmatic-hydrothermal brines (Johnston 1977; Carter et al. 2015; Peretyazhko et al. 2016; Afanasyev et al. 2018); the mineral assemblage found in the volcanic plume of La Soufrière suggests Cl-rich brines circulating in the hydrothermal system interacting with host rocks and magmatic gases containing sulfur. This is supported by the presence of high Cl and S concentrations in gas condensates (Villemant et al. 2014; Inostroza et al. 2022a) and S- and Cl-compounds in the fumarolic gases of La Soufrière (Bernard et al. 2006; Allard et al. 2014; Moretti et al. 2020a, b; Moune et al. 2022). However, the formation mechanism of halide minerals is controversial, and could be explained according to two hypotheses: 1) mineral phases formed at the fumarolic conduit/vent and then transported as solid particles to be subsequently trapped in the aerosol filter, or 2) mineral phases formed because of S- and Cl-rich droplet evaporation during the storage time. Although vent erosion appears as a primary process in La Soufrière emissions, Figures 5 and 6f suggest that the circular distribution of sulfur, sulfates, and Cl-bearing minerals, as well as the delicate and well-formed crystal needles of sulfates and cubic halite, can only be explained by subtle evaporation processes. Furthermore, the clustering of gypsum needles (Fig. 5) agrees with droplet evaporation experiments on hydrophobic surfaces comparable with PTFE filters (Shahidzadeh et al. 2015; Zelenski et al. 2020). Therefore, both hypotheses are plausible, and we suggest that their combination explains the occurrence of halides and sulfates in our samples.

The amount of ash/rock solid particles in magmatic systems can be accounted for by analyzing Rare Earth Elements (REEs) in aerosol filters (Gauthier and Le Cloarec 1998; Aiuppa et al. 2003). REEs are

undoubtedly the indicators of solid particle entrapment due to erosive processes. In addition to particles related to erosive processes, low-temperature emissions also contain acidic hydrothermal solutions enriched in REEs due to variable leaching of the wall rock depending on temperature, pressure, chemical composition, and density of carrier fluids (Karpov et al. 2013; Migdisov et al. 2016; Inguaggiato et al. 2020; Wan et al. 2021). At La Soufrière, plumes show enrichments in REEs lighter than Eu (Fig. 7), same as for gas condensates collected between 2017 and early 2021 (Inostroza et al. 2022a, b). Such Light REE (LREE) enrichments are well correlated with the significant concentrations and degassing of chlorides and sulfates in volcanic emissions, which are the most common ligands for REE. Cl, particularly, is the most enriched element in gas condensates and, therefore, in the hydrothermal reservoir of La Soufrière (Inostroza et al. 2022a), and its presence could be responsible for LREE enrichments given that LREE-chlorides are up to 1.5 times more soluble and stable than Heavy REE (HREE)-chlorides in acid and high-temperature hydrothermal solutions (Migdisov et al. 2016). Such hypothesis is also supported by the acidic, Cl-rich, and high temperature (>250 °C) conditions predominating in the main hydrothermal reservoir beneath La Soufrière summit (Rosas-Carbajal et al. 2016; Moretti et al. 2020a). Besides, the dissolution of sulfates (e.g., jarosite, alunite, or gypsum/anhydrite; Salaün et al., 2011; Heap et al., 2021) in the fumarolic conduit and sulfate-bearing hydrothermally altered andesites could explain part of the enrichment of LREE (Varekamp 2015; Inguaggiato et al. 2020).

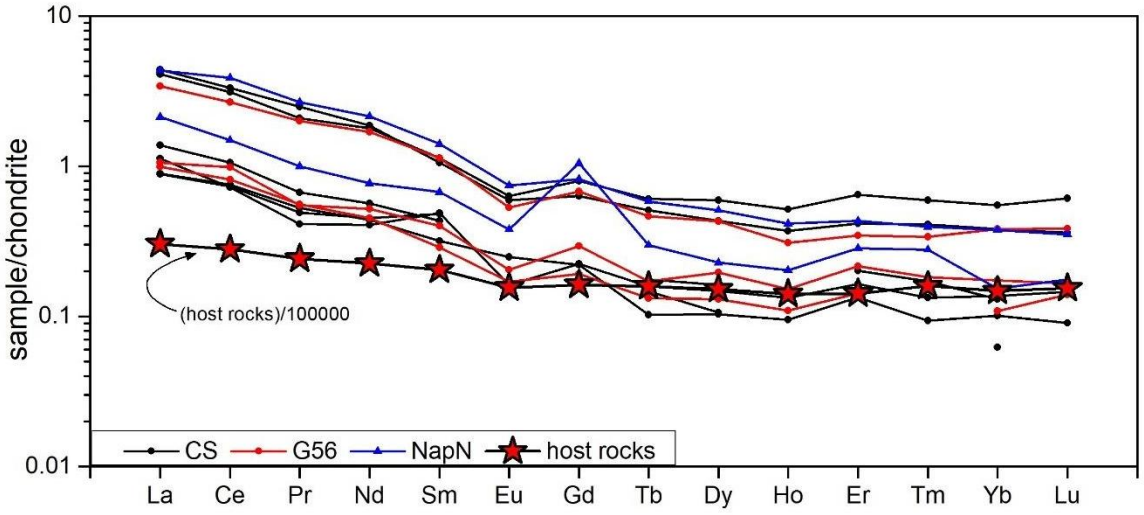

Figure 7 REE patterns normalized to chondrite (Anders and Grevesse 1989) of aerosol filters and andesitic host rocks. REE concentrations in aerosols are those presented in Table 2. In comparison, REE/100000 normalized patterns in andesitic host rocks correspond to the average value of two samples (23CF and SOU-J4) with minimal hydrothermal alteration from the 1530 lava dome and the 1657 scoria fallout deposit presented in Boudon et al. (2008) and Metcalfe et al. (2021), respectively.

5.2 SO_2/H_2S gas ratios

SO_2/H_2S ratios measured by the MultiGas were slightly higher in 2021 with respect to discrete measurements carried out between 2006 and 2020 (Allard et al. 2014; Tamburello et al. 2019; Moune et al.

2022). Nevertheless, filter pack measurements gave even higher ratios (as high as 0.94 in August 2021), up to one order of magnitude higher than the MultiGas dataset (Table 3). These high ratios are considered debatable given SO_2-poor and H_2S-rich plumes at La Soufrière. Such high SO_2 concentrations in filter pack measurements may possibly be because the $NaHCO_3$-impregnated filters could trap S-bearing species other than SO_2 (e.g., H_2S, HS^-, SO_3^{2-}) at high humidity conditions, increasing the concentration of sulfates measured (Mioduszewski and Kress 2008). Therefore, filter wetness could enhance S-species trapping, similar to what occurs in coal industries when alkaline traps are used for H_2S removal (e.g., Garner et al., 1958). Consequently, SO_2 concentrations and SO_2/H_2S gas ratios measured by filter packs in humid and foggy conditions cannot be fully trusted. Nevertheless, H_2S concentrations can be trusted even if some SO_2 is trapped in H_{H2S} filters, which in any case would be minimal given negligible SO_2 concentrations in the plume.

5.3 Trace element enrichment in the plume

Fumarolic plumes at La Soufrière volcano show significant concentrations of major (chemical elements with concentrations above 1000 ppm in host rocks) and trace elements. They include lithophile and siderophile elements, which are well correlated with water-rock interaction in the hydrothermal system and erosive processes in fumarolic conduits, besides chalcophile elements which are usually enriched in volcanic gases given their affinity with sulfur (Symonds et al. 1990; Aiuppa et al. 2003; Inostroza et al. 2022a). Among these, a significant proportion of heavy metals is also present in the plume. The most suitable approach to better understand the volatile and non-volatile contribution of trace elements in volcanic emissions is the enrichment factor (EF; Duce et al. 1975; Mroz and Zoller 1975), which measures the extent of enrichment (or depletion) of an element based on its concentration in host rocks (Lepel et al. 1978; Taran et al. 2001; Gauthier et al. 2016). The EF can be calculated as follow:

$$EF = (X/Y)_a/(X/Y)_r$$

where X and Y are the concentrations of the element of interest and the reference element in the aerosol filter (a) and host rocks (r), respectively. Application of the EF in low-temperature hydrothermal emissions such as those in La Soufrière should be cautiously considered if a comparison with other more magmatic volcanic emissions is intended. Usually, EFs are helpful in better understating magma degassing processes, which explains the frequent application of this method in high-temperature magmatic emissions. In the case of La Soufrière, degassing processes are screened by the extensive hydrothermal system produced by the scavenging of significant but undetermined amount of major and trace elements. Therefore, here we used the EF to evaluate variable contributions related to magma degassing, water-rock interaction, and trace element scavenging.

The choice of the reference element is critical to better interpret EFs; thus an element of low-moderate volatility and of low abundance in andesitic lavas and aerosol filters is commonly used. Be, Mg, Ti, Th, or Br have been commonly chosen as reference elements in earlier EF computations (Symonds et al. 1987;

Taran et al. 1995; Moune et al. 2010; Calabrese et al. 2011; Zelenski et al. 2013), especially in volcanoes with magmatic emissions. However, those reference elements are inappropriate in hydrothermal emissions, given their generally non-negligible concentrations. In our case, Y appears as a good candidate for a reference element, given its low volatility, low concentration in aerosol filters and host rocks, and trusty values according to low RSDs (generally <5 %RSD). Moreover, Y is thoroughly presented in the dataset.

Average Y-based EFs in aerosol samples from CS, G56, and NapN plumes have been presented in Figure 8. Chemical elements enriched in the plume (with EF of 10^3-10^5) are Br, Fe, K, Sb, Ca, Ti, Bi, Si, Cl, Al, Mn, Mg, S, and B. In particular, the enrichment of chalcophiles (Sb, Bi, S) and halogens (e.g., Cl and Br) demonstrate the input of magma-related compounds in the roots of the hydrothermal system (Moune et al. 2010; Allard et al. 2014; Zelenski et al. 2014). Conversely, enrichments in Fe and certain lithophiles evidence the importance of water-rock interaction processes in the volcanic edifice (Symonds et al. 1990; Inostroza et al. 2022a,b). Moreover, Cr, Zn, Sn, Mo, As, I, Ni, Pb, Tl, W, Cu, Cs, and Ta appear moderately enriched in the plume (EF of 10^1-10^3). This group of elements can be interpreted as i) chalcophiles that behave as volatile in magmatic systems, but in La Soufrière, they appear significantly scavenged by volcanic groundwaters, and ii) lithophiles and siderophiles leached from host rocks and transported within aqueous droplets. Finally, a third group poorly enriched in the plume (EF< 10^1) is formed by lithophiles and chalcophiles (except for Ga). These elements can be considered less soluble and are in minor concentrations in both plumes and host rocks of La Soufrière.

In summary, the CS plume shows the highest EF, closely followed by NapN, while the G56 plume occasionally presents EF up to one to two orders of magnitude lower than CS and NapN. Variable EFs at CS, G56, and NapN (Fig. 8) can be explained by, i) artifacts caused by the sampling position and ii) internal magmatic-hydrothermal processes impacting physicochemical characteristics (e.g., flux rates, steam proportion, and outlet temperatures) of fumarolic discharges. We believe that G56 data in this work could be underestimated because of longer sampling distances to the vent and occasionally unfavorable wind direction during sampling, favoring condensation or no collection of certain elements on the filters. On the other hand, CS and NapN offer more appropriate sites for sampling at distances <5 m from the vent.

CS and NapN filters present direct plume exposure, but NapN shows lower EFs than CS (Fig. 8). This variation can be explained based on different degassing processes affecting these fumaroles. For example, it is believed that the transport of major and trace elements in low-temperature fumarolic emissions can be enhanced in the presence of steam-rich fumaroles and high pressure-temperature conditions in the hydrothermal reservoir (Heinrich et al. 1999; Pokrovski et al. 2013). Particularly, NapN differs from CS because of lower steam proportions (75 versus 96 mol%; Tamburello et al. 2019; Moune et al. 2022), lower flux rates (Jessop et al. 2021), and lower outlet temperatures (95 versus 100-111 °C; Moretti et al. 2020a,b; Inostroza et al. 2022a,b). It has been recently demonstrated that NapN emissions are significantly scrubbed by shallow hydrothermal aquifers, while CS preserves a more profound and magmatic signature

(Tamburello et al. 2019; Moretti et al. 2020a). Consequently, the sampling position and physicochemical processes accounting in the magmatic-hydrothermal system play an essential role in the enrichment of major and trace elements in hydrothermal plumes.

Comparison of our computed EF and those recalculated EF from gas condensates collected by Inostroza et al. (2020a; Fig. 8) show a general coherent pattern in plumes and gas condensates, suggesting similar physicochemical processes impacting fumarolic emissions. The main discrepancies are observed in K, Si, Mn, Mg, S, Rb, and Ba, which seem more enriched in condensates than plume measurements, mostly likely due to their transportation within steam condensed droplets or solid particles (Inostroza et al. 2022a) and partial deposition closer to the vent (Sainlot et al. 2020). Gas condensates and plumes from La Soufrière also contain significant concentrations of contaminant trace elements such as Sb, Bi, Cr, As, Ni, Pb, and Tl, some even detected in point-EDS particle analyses (e.g., Cr, Ni). The transport of trace elements in volcanic plumes is usually correlated with the presence of ligands such as halides, sulfates, or hydroxides (Pokrovski et al. 2013; Mandon et al. 2019: Scholtysic and Canil 2020). However, they are characterized by volatility close to zero at the temperatures found in La Soufrière volcano (up to 111 °C) and concentrates in dense and high-temperature brines within the hydrothermal system (Pokrovski et al. 2013). This highlights the important role of water in the transport of metals and metalloids, whose significant concentration in fumarolic emissions is more related to the water-rich concentration rather than the concentration of typical ligands (Pokrovski et al. 2013). Consequently, their transport mechanisms would be linked more to transportation within liquid droplets instead of gaseous compounds (Inostroza et al. 2022a).

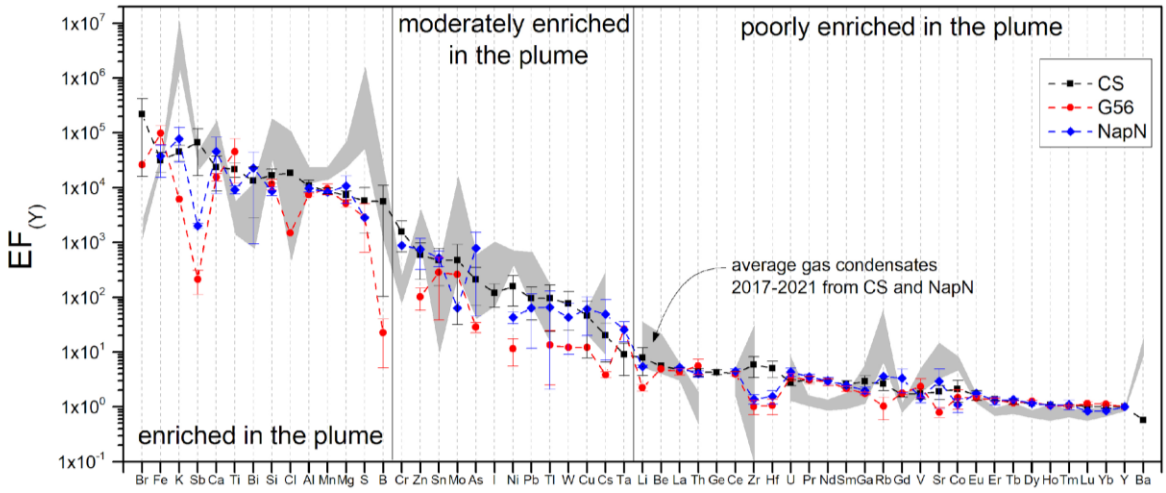

Figure 8 Average Y-based Enrichment Factors (EF_Y) for CS, G56, and NapN plumes. The grey area shows the average EF_Y considering 35 CS and 19 NapN gas condensate samples, respectively, according to the data already published in Inostroza et al. (2022a) (Supplementary Material 2).

5.4 Trace element emission rates at La Soufrière volcano

Any trace element emission rate F(X) can be calculated by multiplying gas-normalized ratios in filter packs by the corresponding gas emission rates (Mather et al. 2004). Typically, SO_2 is the normalization gas species chosen for this calculation because it has an unambiguously magmatic signature, significative concentrations in volcanic plumes, and a wide range of available techniques to measure its concentration. However, SO_2 concentrations are negligible at La Soufrière. Consequently, we calculated emission rates using H_2S fluxes from MultiGas determination in a way similar to Allard et al. (2014), who used this species to estimate La Soufrière's volatile fluxes released from the magma chamber. Their study demonstrated that at La Soufrière, H_2S can be considered as a species of magmatic provenience despite its hydrothermal re-equilibration. Trace element emission rates (F(X)) are then calculated as follows:

$$F(X) = [X/H_2S]_{FP} \times F(H_2S)$$

where $[X/H_2S]_{FP}$ is the mass ratio of any trace element "X" obtained by the filter pack (*FP*) technique and $F(H_2S)$, the H_2S flux measured with the MultiGas.

Trace element emission rates for La Soufrière volcano have been presented in Table 5. These values are computed considering only the selected heavy metals commonly enriched in volcanic plumes and in most cases, originated by magma degassing. The F(X) values (Table 5) have been calculated for four CS and one G56 samples, using H_2S emission rates of 1.50-2.83 and 0.34 t/d, respectively (Table 4). Heavy metal emission rates range from 2.8×10^{-6} to 15 g/d and 1.8×10^{-6} to 6.1 g/d in CS and G56, respectively, with CS samples presenting higher emission rates than the G56 one (Fig. 9) with the exception of Fe, which presents similar emission rates in both CS and G56 plumes. Table 5 and Figure 10 also highlight the high flux of Zn, Ni, and Sb, with emission rates up to ~1 g/d, especially in the sample collected in March 2021. Fe, Zn, Ni, and Sb emission rates are comparable to Hg rates of 2.19 g/d measured at CS in 2006 by Bagnato et al. (2009). Emission rates of Sn, Cu, As, Se, Tl, Pb, Ni, Bi, Te, Co, and Mo generally remained below 0.1 g/d. By comparing CS and G56 fumaroles, it can be shown that Fe, Sn, As, Se, and Co presented relatively similar average emission rates. Conversely, Cu, Zn, Tl, Ni, and Sb appear with emission rates more than one order of magnitude higher in CS, suggesting that the latter trace elements are scrubbed more than Fe, Sn, As, Se, and Co in the hydrothermal system.

These emission rates represent the first data obtained from low-temperature steam-rich volcanic emissions and provide valuable information about the efficiency of trace element scavenging by hydrothermal processes. These emission rates must however be considered as minimum values given possible leaching affecting PTFE filters during sampling in the presence of humid climatic conditions and partial deposition of certain soluble elements near the fumarolic vent (Section 3.1).

Table 5 Trace element emission rates (g/d) discharged from CS and G56 fumaroles in La Soufrière de Guadeloupe volcano. $F(H_2S)$ is the H_2S flux retrieved from MultiGas (in t/d), and H_2S is the concentration (in g/m^3) measured in the aerosol filter using the filter pack technique. Average fluxes in the Caribbean

atmosphere (expressed in t/d) are collected from Chester et al. (1979), Morera-Gómez et al. (2019), and Xu-Yang et al. (2022) and presented in Supplementary Material 3. Atmospheric fluxes are converted from kg m^{-2} y^{-1} into kg/d using the areal factor of 35±5 m^2, which corresponds to the average plume cross-section considering a flattened plume of 3-4 m high and 10 m wide (Gaudin et al., 2016; Allard et al., 2016; Jessop et al., 2021; Moune et al., 2022).

Fumarole	**CS**	**CS**	**CS**	**CS**	**G56**	**Caribbean Atmosphere ***
Filter	**H_{H2S}**	**H_A**	**H_A**	**H_A**	**H_A**	-
Date	**16/03/2021**	**04/06/2021**	**15/06/2021**	**25/08/2021**	**19/07/2021**	-
F(H_2S)	1.50	2.83	2.83	1.57	0.34	-
H_2S	0.16	1.67	1.11	1.05	0.58	-
Fe	1.4×10^{-1}	2.5×10^{0}	1.5×10^{1}	9.2×10^{0}	6.1×10^{0}	4.0×10^{-2}
Cr	4.4×10^{0}	1.3×10^{-1}	2.2×10^{-2}	nd	nd	1.0×10^{-4}
Sn	2.7×10^{-4}	4.4×10^{-2}	3.1×10^{-3}	5.2×10^{-2}	7.2×10^{-3}	1.2×10^{-5}
Cu	1.5×10^{-2}	2.0×10^{-1}	2.1×10^{-2}	6.3×10^{-2}	4.8×10^{-3}	1.8×10^{-4}
As	nd	3.0×10^{-3}	1.6×10^{-3}	2.1×10^{-3}	2.7×10^{-4}	4.2×10^{-5}
Zn	1.1×10^{0}	2.3×10^{0}	5.1×10^{-2}	8.9×10^{-1}	3.5×10^{-2}	1.5×10^{-3}
Se	2.8×10^{-2}	6.7×10^{-4}	nd	2.3×10^{-3}	1.3×10^{-3}	nd
Tl	2.1×10^{-3}	2.8×10^{-6}	1.9×10^{-5}	2.6×10^{-5}	1.8×10^{-6}	4.6×10^{-7}
Pb	6.1×10^{-3}	8.4×10^{-3}	nd	4.1×10^{-3}	nd	1.3×10^{-4}
Ni	2.7×10^{-1}	8.1×10^{-2}	4.4×10^{-3}	8.9×10^{-3}	1.5×10^{-3}	9.2×10^{-5}
Bi	nd	3.1×10^{-4}	nd	1.3×10^{-5}	Nd	9.8×10^{-5}
Sb	1.7×10^{0}	1.7×10^{-2}	4.0×10^{-1}	1.5×10^{-2}	1.0×10^{-4}	8.1×10^{-5}
Te	nd	3.5×10^{-5}	2.9×10^{-4}	1.1×10^{-4}	nd	nd
Co	7.3×10^{-3}	7.7×10^{-4}	2.0×10^{-3}	1.3×10^{-3}	2.7×10^{-4}	1.0×10^{-5}
Mo	4.8×10^{-2}	4.8×10^{-4}	nd	7.4×10^{-4}	nd	1.1×10^{-5}

Nd: not determined/not calculated

Comparing La Soufrière emission rates with other quiescently degassing subduction-related volcanoes permits a better understanding of the heavy metal contribution at this volcano and low-temperature hydrothermal emissions. Figure 9 shows that La Soufrière's emissions rates are the lowest values reported in the limited literature data for magmatic-hydrothermal emissions. Typical magmatic emissions range between 1 and 2500 kg/d (Moune et al. 2010; Allard et al., 2016), while magmatic-hydrothermal systems such as Lascar (Chile), White Island (New Zealand), and El Chichon (Mexico) emit heavy metal rates ranging from 0.004 to 220 kg/d (Phelan Kotra et al. 1983; Menard et al. 2014; Mandon et al. 2019). Emission rates of <15 g/d at La Soufrière (Table 5) represent a modest contribution compared to global heavy metal emission rates in actively degassing volcanoes. Such differences can be explained based on variable magmatic and hydrothermal contributions depending on the depth of magma mush and the amount of water inside the volcano edifice. Higher emission rates are well correlated with a more significant magmatic contribution of heavy metals that are degassed directly from shallow crustal magma chambers, as typically observed at volcanoes that have experienced recent magmatic eruptions, such as El

Chichon or White Island (Global Volcanism Program 2022), and also at open vent volcanoes such as Masaya and Ambrym. We suggest that low emission rates of heavy metals observed at La Soufrière and Lascar can be attributed to the depth of the magma chamber, which in both is located at >6 km below the volcano summit (Díaz et al. 2012; Pichavant et al. 2018). Such considerable depths favor the interaction of heavy metals with host rocks and groundwaters on their rise through the conduit system. Despite similar magma chamber depths beneath La Soufrière and Lascar, these volcanoes differ in the amount of rainwater entering in their hydrothermal systems. For example, Lascar is located in the driest desert on the Earth, while La Soufrière is impacted by huge inputs of rainwater (up to 10 m per year; Dessert et al. 2015). Such an input favors widespread hydrothermal emissions at La Soufrière, supported by the predominance of H_2S instead of SO_2, including numerous cold and thermal emissions on volcano flanks. On the other hand, Lascar presents fumarolic emissions rich in SO_2, HF, and HCl (Mather et al. 2004; Tassi et al. 2009), and a few thermal springs, and reports of subplinian and vulcanian eruptions in the last decades (Matthews et al. 1997; Global Volcanism Program 2013). Consequently, it is believed that low heavy metal emissions rates at La Soufrière and other low-temperature volcanic emissions are strongly influenced by the location of the magma chamber and the extent of scrubbing processes depending on the amount of water inside the volcanic edifice (Blundy et al. 2021).

Computed heavy metal fluxes were then compared to average Caribbean atmospheric deposition fluxes reported in Chester et al. (1979), Morera-Gómez et al. (2019), and Xu-Yang et al. (2022) to estimate if volcanic emissions from La Soufrière represent an important pollution source in the Caribbean atmosphere. Deposition fluxes represent the amount of material that is deposited in a given area and period of time, without considering chemical species that remain in the atmosphere Thus these fluxes represent only a fraction of the elements in the Caribbean atmosphere and should be considered as a minimum. Average fluxes were used being aware that the Caribbean atmosphere presents heterogeneities in terms of heavy metal content along the Lesser Antilles arc. Furthermore, Morera-Gomez et al. (2019) found anthropogenic influence in Cuba. However, Fe and Zn fluxes (Supplementary Material 3), which are elements sensitive to anthropogenic contamination, suggest relatively homogeneous atmospheric chemical composition at the time of these studies. This allowed us to ensure the consistency of the heavy metal data we used for comparison.

Atmospheric fluxes have been converted into kg/d using the areal factor of 35±5 m^2, which corresponds to the average plume cross-section considering a flattened plume of 3-4 m high and 10 m wide, following the observations made by Allard et al. (2014), Gaudin et al. (2016), Jessop et al. (2021) and Moune et al. (2022). Successively, normalized fluxes ranged between 4.6×10^{-10} and 4.0×10^{-5} kg/d (Fig. 9). These atmospheric fluxes are up to four times lower (e.g., Cr, Sb, Sn, Mo) than La Soufrière fluxes, especially in the case of the CS fumarole, which is considered as the primary heavy metal source at this volcano. Notably, atmospheric and volcanic fluxes of Bi displayed closer values, while the G56 fumarole has average fluxes equal to or slightly higher than atmospheric fluxes. Consequently, modest heavy metal emissions from La Soufrière can be regarded as a source of pollution in Guadeloupe, although their impact

are very limited in space compared to the major contributors such as dust from the Sahara and marine salts. Moreover, anthropogenic inputs remain poorly constrained and should be carefully considered in future studies, although their influence is believed to be minimal.

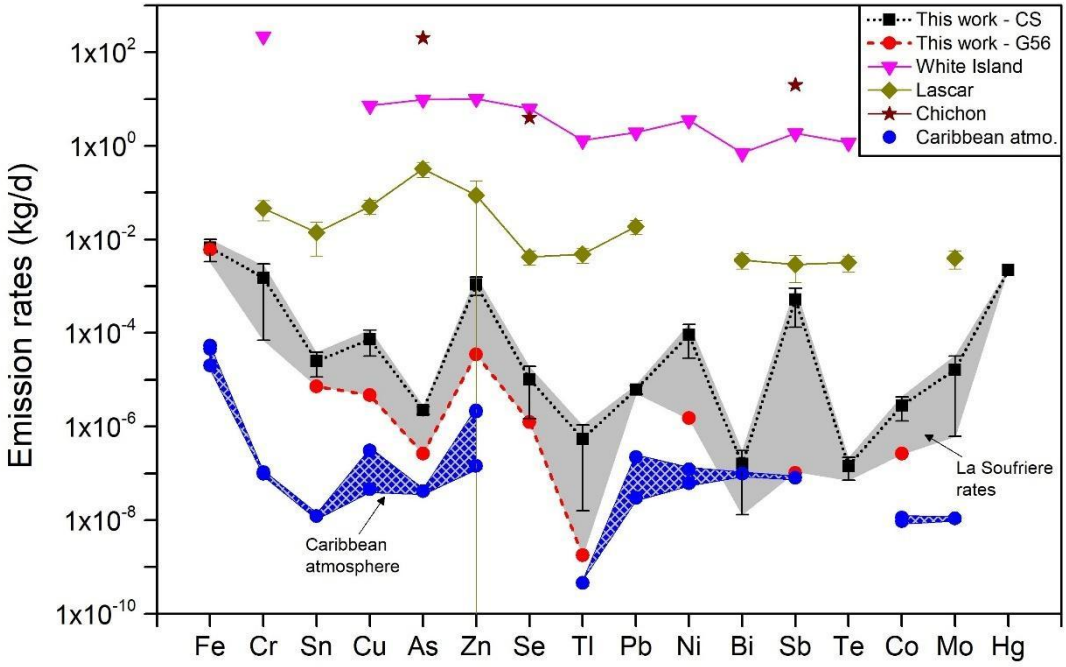

Figure 9 Heavy metal emission rates (kg/d) compared with other subduction-related and quiescently degassing volcanoes with evidence of hydrothermal activity, such as White Island (Mandon et al. 2019), Lascar (Menard et al. 2014), and El Chichon (Phelan Kotra et al. 1983) volcanoes. The gray area represents emission rates at La Soufrière, and the black dotted and red dashed lines are average emission rates from CS and G56 fumaroles, respectively. The blue dashed area represents the average trace element deposition fluxes in the Caribbean atmosphere according to published bibliographic data (Chester et al. 1979; Morera-Gómez et al. 2019; Xu-Yang et al. 2022).

6 CONCLUSIONS

This work presented a detailed study on the physicochemical characteristics of volcanic plumes from Cratere Sud, Napoleon Nord, and Gouffre 56 fumaroles, three of the most important degassing sites in La Soufrière de Guadeloupe volcano. The sampling was challenging because of harsh weather conditions on the volcano summit and the nature (steamy- and H_2S-rich) of fumarolic emissions, forcing the adaptation of traditional sampling procedures. Given these distinctive characteristics, aerosol filters developed droplets during exposure to the plume, following which the partial leaching potentially occurred. Consequently, major and trace element concentrations in the analyzed plumes must be considered minimum concentrations.

Microscopic and chemical analyses identified major and trace elements transported within gas and aerosol phases. Remarkably, volcanic plumes at La Soufrière contain significant concentrations of lithophile or rock-related elements from water-rock interaction processes in the hydrothermal system, in addition to significant concentrations of chalcophiles related to a deeper magmatic source. Moreover, La Soufrière is an important source of potentially toxic heavy metals such as Sb, Bi, Cr, As, Ni, Pb, and Tl. Given low outlet gas temperatures at La Soufrière's vents, it is believed that most of the elements enriched in the plume are transported within tiny droplets, although the presence of Si-rich and sulfur particles suggests the substantial erosion at the vent. Rock-related and chalcophile elements suggest a variable contribution from hydrothermal sources and magmatic degassing processes.

This work also presents the first estimate of heavy metal emission rates discharged at La Soufrière fumaroles. Modest emissions rates (up to 15 g/d) are ascribed to the combination of two physicochemical factors: 1) low-temperature fumarolic emissions and 2) small amount of common heavy metal ligands such as chlorides and sulfates in the gas phase. These factors can be explained by a relatively deep location of the magma chamber, the primary source of heavy metals, and the presence of a well-developed hydrothermal system in the volcanic edifice fed by abundant rainfall typical of tropical environments. We suggest that these factors may occur at other volcanoes at the hydrothermal stage whose fluids have a clear magmatic signature. Estimated heavy metal emission rates place La Soufrière as the most modest heavy metal emitter among quiescently degassing subduction volcanoes, but still as an important point of pollution in the Lesser Antilles volcanic arc. Heavy metal degassing at La Soufrière suggests no evident hazard at the volcano summit. However, additional research should be carried out about the transport and evolution of species in low-temperature volcanic plumes released in tropical environments to evaluate their impact on nearby communities.

ACKNOWLEDGMENTS

We thank the FEDER FSE PO and the IPGP for their recurrent funding to the Observatoires Volcanologiques et Sismologiques (OVS-IPGP), the INSU-CNRS for funding provided by Service National d'Observation en Volcanologie (SNOV), and the Office de l'Eau Guadeloupe via the OVSG/IPGP-OE971 agreement. We also thank Yves Bercion and Fabienne Zami from the C3 MAG laboratory at the Université des Antilles and Stephan Borensztajn from the IPGP for assistance during SEM analyses. ICP-MS analyses were supported by IPGP multidisciplinary program PARI, and Paris-IdF region SESAME Grant n° 12015908. Finally, we also thank Chantal Bosq (UCA), who facilitated the use of the clean room at LVM.

FUNDING STATEMENT

This work was supported by the EU-funded project IMMERGE (Impact multi-environnemental des retombées volcaniques et sahariennes en Guadeloupe; PI: Céline Dessert, IPGP). This project has been financially supported by European (FEDER FSE PO 2014–2020) and Région Guadeloupe funding

(agreement GP0023419). RM acknowledges financial support from the project INSU-CNRS Tellus-Aléas "Unrest", year 2021. This study contributes to the IdEx Université de Paris ANR-18-IDEX-0001 and the Laboratory of excellence ClerVolc number 589.

SUPPLEMENTARY MATERIALS

Supplementary Material 1 provides all SEM-EDS images, including the location of point-chemical analyses. Supplementary Material 2 corresponds to an excel file including chemical and background corrections, besides EF computations. Finally, Supplementary Material 3 provides general information and computations concerning filter packs, MultiGas, and trace element fluxes.

CONFLICTS OF INTEREST

The authors declare there are no conflicts of interest.

REFERENCES

Afanasyev A, Blundy J, Melnik O, Sparks S (2018) Formation of magmatic brine lenses via focussed fluid-flow beneath volcanoes. Earth Planet Sc Lett 486:119–128. https://doi.org/10.1016/j.epsl.2018.01.013

Africano F, Bernard A (2000) Acid alteration in the fumarolic environment of Usu volcano, Hokkaido, Japan. J Volcanol Geoth Res 97:475–495. https://doi.org/10.1016/S0377-0273(99)00162-6

Africano F, Van Rompaey G, Bernard A, Le Guern F (2002) Deposition of trace elements from high temperature gases of Satsuma-Iwojima volcano. Earth Planet Sp 54:275–286. https://doi.org/10.1186/BF03353027

Aguilera F, Layana S, Rodríguez-Díaz A, et al (2016) Hydrothermal alteration, fumarolic deposits and fluids from Lastarria Volcanic Complex: A multidisciplinary study. Andean Geol 43:166. https://doi.org/10.5027/andgeoV43n2-a02

Aiuppa A, Dongarrà G, Valenza M, et al (2003) Degassing of trace volatile metals during the 2001 eruption of Etna. In: Robock A, Oppenheimer C (eds) Geophysical Monograph Series. American Geophysical Union, Washington, D. C., pp 41–54

Aiuppa A, Federico C, Giudice G, Gurrieri S (2005a) Chemical mapping of a fumarolic field: La Fossa Crater, Vulcano Island (Aeolian Islands, Italy). Geophys Res Lett 32:L13309. https://doi.org/10.1029/2005GL023207

751 Aiuppa A, Fischer T, Plank T, et al (2017) Along-arc, inter-arc and arc-to-arc variations in volcanic gas
752 CO2/ST ratios reveal dual source of carbon in arc volcanism. Earth-Sci Rev 168:24–47.
753 https://doi.org/10.1016/j.earscirev.2017.03.005

754 Aiuppa A, Inguaggiato S, McGonigle AJS, et al (2005b) H2S fluxes from Mt. Etna, Stromboli, and
755 Vulcano (Italy) and implications for the sulfur budget at volcanoes. Geochim Cosmochim Ac 69:1861–
756 1871. https://doi.org/10.1016/j.gca.2004.09.018

757 Allard P, Aiuppa A, Bani P, et al (2016) Prodigious emission rates and magma degassing budget of major,
758 trace and radioactive volatile species from Ambrym basaltic volcano, Vanuatu island Arc. J Volcanol
759 Geoth Res 322:119–143. https://doi.org/10.1016/j.jvolgeores.2015.10.004

760 Allard P, Aiuppa A, Beauducel F, et al (2014) Steam and gas emission rate from La Soufrière volcano,
761 Guadeloupe (Lesser Antilles): Implications for the magmatic supply during degassing unrest. Chem Geol
762 384:76–93. https://doi.org/10.1016/j.chemgeo.2014.06.019

763 Allen AG, Baxter PJ, Ottley CJ (2000) Gas and particle emissions from Soufrière Hills Volcano,
764 Montserrat, West Indies: characterization and health hazard assessment. B Volcanol 62:8–19.
765 https://doi.org/10.1007/s004450050287

766 Anders E, Grevesse N (1989) Abundances of the elements: Meteoritic and solar. Geochim Cosmochim Ac
767 53:197–214. https://doi.org/10.1016/0016-7037(89)90286-X

768 Badocco D, Romanini F, Di Marco V, Mondin A, Pastore P (2017) Formation of volatile iodine
769 compounds under hot concentrated acid conditions (nitric acid or aqua regia) and in diluted acid solutions
770 with or without thiocyanate. Polyhedron, 122, 25-28

771 Bagnato E, Tamburello G, Avard G, et al (2015) Mercury fluxes from volcanic and geothermal sources: an
772 update. Geol Soc Spec Publ 410:263–285. https://doi.org/10.1144/SP410.2

773 Bernard M-L, Molinié J, Petit R-H, et al (2006) Remote and in situ plume measurements of acid gas
774 release from La Soufrière volcano, Guadeloupe. J Volcanol Geoth Res 150:395–409.
775 https://doi.org/10.1016/j.jvolgeores.2005.08.001

776 Blundy J, Afanasyev A, Tattitch B, Sparks S, Melnik O, Utkin I, Rust A (2021) The economic potential of
777 metalliferous sub-volcanic brines. Roy Soc Open Sci, 8(6), 202192.

778 Boudon G, Komorowski J-C, Villemant B, Semet MP (2008) A new scenario for the last magmatic
779 eruption of La Soufrière of Guadeloupe (Lesser Antilles) in 1530 A.D. Evidence from stratigraphy
780 radiocarbon dating and magmatic evolution of erupted products. J Volcanol Geoth Res 178:474–490.
781 https://doi.org/10.1016/j.jvolgeores.2008.03.006

Brombach T, Marini L, Hunziker JC (2000) Geochemistry of the thermal springs and fumaroles of Basse-Terre Island, Guadeloupe, Lesser Antilles. Bull Volcanol 61:477–490. https://doi.org/10.1007/PL00008913

Calabrese S, Aiuppa A, Allard P, et al (2011) Atmospheric sources and sinks of volcanogenic elements in a basaltic volcano (Etna, Italy). Geochim Cosmochim Ac 75:7401–7425. https://doi.org/10.1016/j.gca.2011.09.040

Carter J, Viviano-Beck C, Loizeau D, et al (2015) Orbital detection and implications of akaganéite on Mars. Icarus 253:296–310. https://doi.org/10.1016/j.icarus.2015.01.020

Chabas A, Lefèvre RA (2000) Chemistry and microscopy of atmospheric particulates at Delos (Cyclades–Greece). Atmospheric Environment 34:225–238. https://doi.org/10.1016/S1352-2310(99)00255-1

Chen J-B, Gaillardet J, Dessert C, et al (2014) Zn isotope compositions of the thermal spring waters of La Soufrière volcano, Guadeloupe Island. Geochim Cosmochim Ac 127:67–82. https://doi.org/10.1016/j.gca.2013.11.022

Chen, C.T.A., Zeng, Z., Kuo, F.W., Yang, T.F., Wang, B.J., & Tu, Y.Y. (2005). Tide-influenced acidic hydrothermal system offshore NE Taiwan. Chem Geol, 224(1-3), 69-81.

Chester, R., Griffiths, A. G., & Hirst, J. M. (1979). The influence of soil-sized atmospheric particulates on the elemental chemistry of the deep-sea sediments of the northeastern Atlantic. Mar Geol 32(1-2), 141-154.

Crowe BM, Finnegan DL, Zoller WH, Boynton WV (1987) Trace element geochemistry of volcanic gases and particles from 1983-1984 eruptive episodes of Kilauea Volcano. J Geophys Res 92:13708–13714. https://doi.org/10.1029/JB092iB13p13708

de Bremond d'Ars J, Gibert D (2022) Low-Temperature Hydrothermal Systems Response to Rainfall Forcing: An Example From Temperature Time Series of Fumaroles at La Soufrière de Guadeloupe Volcano. Front Earth Sci 9:772176. https://doi.org/10.3389/feart.2021.772176

Deng Q, Yin J, Wu X, et al (2019) Research Advances of Prevention and Control of Hydrogen Sulfide in Coal Mines. The Scientific World Journal 2019:1–15. https://doi.org/10.1155/2019/8719260

Dessert C, Clergue C, Rousteau A, Crispi O, Benedetti MF. (2020). Atmospheric contribution to cations cycling in highly weathered catchment, Guadeloupe (Lesser Antilles). Chemical Geology, 531, 119354. https://doi.org/10.1016/j.chemgeo.2019.119354

811 Dessert C, Lajeunesse E, Lloret E, et al (2015) Controls on chemical weathering on a mountainous
812 volcanic tropical island: Guadeloupe (French West Indies). Geochim Cosmochim Ac 171:216–237.
813 https://doi.org/10.1016/j.gca.2015.09.009

814 Díaz D, Brasse H, Ticona F (2012) Conductivity distribution beneath Lascar volcano (Northern Chile) and
815 the Puna, inferred from magnetotelluric data. J Volcanol Geoth Res 217–218:21–29.
816 https://doi.org/10.1016/j.jvolgeores.2011.12.007

817 Duce RA, Hoffman GL, Zoller WH (1975) Atmospheric Trace Metals at Remote Northern and Southern
818 Hemisphere Sites: Pollution or Natural? Science 187:59–61. https://doi.org/10.1126/science.187.4171.59

819 Dusek, U., Frank, G.P., Hildebrandt, L., Curtius, J., Schneider, J., Walter, S., Chand, D., Drewnick, F.,
820 Hings, S., Jung, D., Borrman, S., Andreae, M.O. (2006). Size matters more than chemistry for cloud-
821 nucleating ability of aerosol particles. Science, 312(5778), 1375-1378.

822 Euphrasie-Clotilde L, Plocoste T, Brute F-N (2021) Particle Size Analysis of African Dust Haze over the
823 Last 20 Years: A Focus on the Extreme Event of June 2020. Atmosphere 12:502.
824 https://doi.org/10.3390/atmos12040502

825 Feuillet, N., Manighetti, I., Tapponnier, P., Jacques, E. (2002). Arc parallel extension and localization of
826 volcanic complexes in Guadeloupe, Lesser Antilles. Journal of Geophysical Research: Solid Earth,
827 107(B12), ETG-3. https://doi.org/10.1029/2001JB000308

828 Finnegan DL, Kotra JP, Hermann DM, Zoller WH (1989) The use of7LiOH-impregnated filters for the
829 collection of acidic gases and analysis by instrumental neutron activation analysis. Bull Volcanol 51:83–
830 87. https://doi.org/10.1007/BF01081977

831 Fischer T, Chiodini G (2015) Volcanic, Magmatic and Hydrothermal Gases. In: The Encyclopedia of
832 Volcanoes. Elsevier, pp 779–797

833 Garner FH, Long R, Pennell A (1958) The selective absorption of hydrogen sulphide in carbonate
834 solutions. J Appl Chem 8:325–336. https://doi.org/10.1002/jctb.5010080509

835 Gaudin D, Beauducel F, Coutant O, et al (2016) Mass and heat flux balance of La Soufrière volcano
836 (Guadeloupe) from aerial infrared thermal imaging. J Volcanol Geoth Res 320:107–116.
837 https://doi.org/10.1016/j.jvolgeores.2016.04.007

838 Gauthier P-J, Le Cloarec M-F (1998) Variability of alkali and heavy metal fluxes released by Mt. Etna
839 volcano, Sicily, between 1991 and 1995. J Volcanol Geotherm Res 81:311–326.
840 https://doi.org/10.1016/S0377-0273(98)00002-X

Gauthier P-J, Sigmarsson O, Gouhier M, et al (2016) Elevated gas flux and trace metal degassing from the 2014-2015 fissure eruption at the Bárðarbunga volcanic system, Iceland: Degassing at Holuhraun. J Geophys Res Solid Earth 121:1610–1630. https://doi.org/10.1002/2015JB012111

Getahun A, Reed MH, Symonds R (1996) Mount St. Augustine volcano fumarole wall rock alteration: mineralogy, zoning, composition and numerical models of its formation process. J Volcanol Geoth Res 71:73–107. https://doi.org/10.1016/0377-0273(95)00071-2

Giggenbach WF (1996) Chemical Composition of Volcanic Gases. In: Monitoring and Mitigation of Volcano Hazards. Springer Berlin Heidelberg, Berlin, Heidelberg, pp 221–256

Global Volcanism Program (2013) Volcanoes of the World, v. 4.3.4

Goldschmidt VM (1937) The principles of distribution of chemical elements in minerals and rocks. The seventh Hugo Müller Lecture, delivered before the Chemical Society on March 17th, 1937. J Chem Soc 0:655–673. https://doi.org/10.1039/JR9370000655

Heap MJ, Baumann TS, Rosas- Carbajal M, et al (2021) Alteration- Induced Volcano Instability at La Soufrière de Guadeloupe (Eastern Caribbean). J Geophys Res Solid Earth 126:. https://doi.org/10.1029/2021JB022514

Heinrich CA, Günther D, Audétat A, et al (1999) Metal fractionation between magmatic brine and vapor, determined by microanalysis of fluid inclusions. Geol 27:755. https://doi.org/10.1130/0091-7613(1999)027<0755:MFBMBA>2.3.CO;2

Hincks TK, Komorowski J-C, Sparks SR, Aspinall WP (2014) Retrospective analysis of uncertain eruption precursors at La Soufrière volcano, Guadeloupe, 1975–77: volcanic hazard assessment using a Bayesian Belief Network approach. J Appl Volcanol 3:3. https://doi.org/10.1186/2191-5040-3-3

Inguaggiato C, Pérez García MÁ, Meza Maldonado LF, et al (2020) Precipitation of secondary minerals in acid sulphate-chloride waters traced by major, minor and rare earth elements in waters: The case of Puracé volcano (Colombia). J Volcanol Geoth Res 407:107106. https://doi.org/10.1016/j.jvolgeores.2020.107106

Inostroza M, Moune S, Moretti R, et al (2022a) Decoding water-rock interaction and volatile input at La Soufrière volcano (Guadeloupe) using time-series major and trace element analyses in gas condensates. J Volcanol Geoth Res 425:107517. https://doi.org/10.1016/j.jvolgeores.2022.107517

Inostroza M, Moune S, Moretti R, et al (2022b) Monitoring Hydrothermal Activity Using Major and Trace Elements in Low-Temperature Fumarolic Condensates: The Case of La Soufrière de Guadeloupe Volcano. Geosciences 12:267. https://doi.org/10.3390/geosciences12070267

871 Jessop D, Moune S, Moretti R, et al (2021) A multi-decadal view of the heat and mass budget of a volcano
872 in unrest: La Soufrière de Guadeloupe (French West Indies). Bull Volcanol 83:16.
873 https://doi.org/10.1007/s00445-021-01439-2

874 Jian L, Goessler W, Irgolic KJ (2000) Mercury determination with ICP-MS: signal suppression by acids.
875 Fresen J Anal Chem, 366, 48-53

876 Johnston JH (1977) Jarosite and akaganéite from White Island volcano, New Zealand: An X-ray and
877 Mössbauer study. Geochim Cosmochim Ac 41:539–544. https://doi.org/10.1016/0016-7037(77)90291-5

878 Karpov GA, Nikolaeva AG, Alekhin YuV (2013) Abundances and sources of rare-earth elements in the
879 modern volcanogenic hydrothermal systems of Kamchatka. Petrology 21:145–157.
880 https://doi.org/10.1134/S0869591113020045

881 Komorowski J-C, Boudon G, Semet MP, Beauducel F (2005) Volcanic hazard atlas of the Lesser Antilles:
882 Guadeloupe. In: Volcanic hazard atlas of the Lesser Antilles

883 Legendre Y (2012) Reconstruction de l'histoire éruptive et scenarii éruptifs à La Soufrière de Guadeloupe:
884 vers un modèle intégrale de fonctionnement du volcan. (French) [A high resolution reconstruction of the
885 eruptive past and definition of eruptive scenario at La Soufrière of Guadeloupe]. Ph.D. Thesis, Université
886 Paris 7

887 Lepel EA, Stefansson KM, Zoller WH (1978) The enrichment of volatile elements in the atmosphere by
888 volcanic activity: Augustine volcano 1976. J Geophys Res 83:6213.
889 https://doi.org/10.1029/JC083iC12p06213

890 Mandon CL, Christenson BW, Schipper CI, et al (2019) Metal transport in volcanic plumes: A case study
891 at White Island and Yasur volcanoes. J Volcanol Geotherm Res 369:155–171.
892 https://doi.org/10.1016/j.jvolgeores.2018.11.024

893 Mather TA (2015) Volcanoes and the environment: Lessons for understanding Earth's past and future from
894 studies of present-day volcanic emissions. J Volcanol Geotherm Res 304, 160-179.
895 https://doi.org/10.1016/j.jvolgeores.2015.08.016

896 Mather TA, Allen AG, Davison BM, et al (2004) Nitric acid from volcanoes. Earth Planet Sci Lett 218:17–
897 30. https://doi.org/10.1016/S0012-821X(03)00640-X

898 Mather TA, Pyle D.M, Oppenheimer C (2003) Tropospheric volcanic aerosol. Geophys Monogr 139, 189-
899 212. https://doi.org/10.1029/139GM12

Matthews SJ, Gardeweg MC, Sparks RSJ (1997) The 1984 to 1996 cyclic activity of Lascar Volcano, northern Chile: cycles of dome growth, dome subsidence, degassing and explosive eruptions. Bull Volcanol 59:72–82. https://doi.org/10.1007/s004450050176

Menard G, Moune S, Vlastélic I, et al (2014) Gas and aerosol emissions from Lascar volcano (Northern Chile): Insights into the origin of gases and their links with the volcanic activity. J Volcanol Geotherm Res 287:51–67. https://doi.org/10.1016/j.jvolgeores.2014.09.004

Metcalfe A, Moune S, Komorowski J-C, et al (2021) Magmatic Processes at La Soufrière de Guadeloupe: Insights From Crystal Studies and Diffusion Timescales for Eruption Onset. Front Earth Sci 9:617294. https://doi.org/10.3389/feart.2021.617294

Migdisov A, Williams-Jones AE, Brugger J, Caporuscio FA (2016) Hydrothermal transport, deposition, and fractionation of the REE: Experimental data and thermodynamic calculations. Chem Geol 439:13–42. https://doi.org/10.1016/j.chemgeo.2016.06.005

Mioduszewski L, Kress V (2008) Laboratory calibration of chemical volcanic gas sampling techniques using an artificial fumarole. J Volcanol Geoth Res 174:295–306. https://doi.org/10.1016/j.jvolgeores.2008.02.006

Morera-Gómez Y, Santamaría JM, Elustondo D, et al (2019) Determination and source apportionment of major and trace elements in atmospheric bulk deposition in a Caribbean rural area. Atmos Environ 202:93–104. https://doi.org/10.1016/j.atmosenv.2019.01.019

Moretti R, Komorowski J-C, Ucciani G, et al (2020a) The 2018 unrest phase at La Soufrière of Guadeloupe (French West Indies) andesitic volcano: Scrutiny of a failed but prodromal phreatic eruption. J Volcanol Geoth Res 393:106769. https://doi.org/10.1016/j.jvolgeores.2020.106769

Moretti R, Moune S, Robert V, et al (2020b) Intercomparison of geochemical techniques at La Soufrière de Guadeloupe (FWI) volcano: their advantages and their limits over a long-standing unrest. Ital J Geosci 139:398–412. https://doi.org/10.3301/IJG.2020.13

Moretti R, Stefánsson A (2020) Volcanic and Geothermal Redox Engines. Elements 16:179–184. https://doi.org/10.2138/gselements.16.3.179

Moune S, Gauthier P-J, Delmelle P (2010) Trace elements in the particulate phase of the plume of Masaya Volcano, Nicaragua. J Volcanol Geoth Res 193:232–244. https://doi.org/10.1016/j.jvolgeores.2010.04.004

Moune S, Moretti R, Burtin A, et al (2022) Gas Monitoring of Volcanic-Hydrothermal Plumes in a Tropical Environment: The Case of La Soufrière de Guadeloupe Unrest Volcano (Lesser Antilles). Front Earth Sci 10:795760. https://doi.org/10.3389/feart.2022.795760

931 Mroz EJ, Zoller WH (1975) Composition of Atmospheric Particulate Matter from the Eruption of
932 Heimaey, Iceland. Science 190:461–463. https://doi.org/10.1126/science.190.4213.461

933 Muhs DR, Bush CA, Stewart KC, et al (1990) Geochemical Evidence of Saharan Dust Parent Material for
934 Soils Developed on Quaternary Limestones of Caribbean and Western Atlantic Islands. Quat res 33:157–
935 177. https://doi.org/10.1016/0033-5894(90)90016-E

936 Murphy DM, Froyd KD, Bian H, et al (2019) The distribution of sea-salt aerosol in the global troposphere.
937 Atmos Chem Phys 19:4093–4104. https://doi.org/10.5194/acp-19-4093-2019

938 Natusch D, Klonis H, Axelrod H, et al (1972) Sensitive method for measurement of atmospheric hydrogen
939 sulfide. Anal Chem 44:2067–2070

940 Nekvasil H, DiFrancesco NJ, Rogers AD, et al (2019) Vapor- deposited minerals contributed to the
941 martian surface during magmatic degassing. J Geophys Res Planets 2018JE005911.
942 https://doi.org/10.1029/2018JE005911

943 Obenholzner JH, Schroettner H, Golob P, Delgado H (2003) Particles from the plume of Popocatépetl
944 volcano, Mexico—the FESEM/EDS approach. Geological Society, London, Special Publications, 213(1),
945 123-148.

946 O'Dowd CD, de Leeuw G (2007) Marine aerosol production: a review of the current knowledge. Phil
947 Trans R Soc A 365:1753–1774. https://doi.org/10.1098/rsta.2007.2043

948 Pennisi M, Le Cloarec M-F (1998) Variations of Cl, F, and S in Mount Etna's plume, Italy, between 1992
949 and 1995. J Geophys Res 103:5061–5066. https://doi.org/10.1029/97JB03011

950 Peretyazhko TS, Fox A, Sutter B, et al (2016) Synthesis of akaganeite in the presence of sulfate:
951 Implications for akaganeite formation in Yellowknife Bay, Gale Crater, Mars. Geochim Cosmochim Ac
952 188:284–296. https://doi.org/10.1016/j.gca.2016.06.002

953 Petit RH (2005) Transport of Saharan dust over the Caribbean Islands: Study of an event. J Geophys Res
954 110:D18S09. https://doi.org/10.1029/2004JD004748

955 Phelan Kotra J, Finnegan DL, Zoller WH, et al (1983) El Chichón: Composition of Plume Gases and
956 Particles. Science 222:1018–1021. https://doi.org/10.1126/science.222.4627.1018

957 Pichavant M, Poussineau S, Lesne P, et al (2018) Experimental Parametrization of Magma Mixing:
958 Application to the ad 1530 Eruption of La Soufrière, Guadeloupe (Lesser Antilles). J Petrol 59:257–282.
959 https://doi.org/10.1093/petrology/egy030

960 Pokrovski GS, Borisova AY, Bychkov AY (2013) Speciation and Transport of Metals and Metalloids in
961 Geological Vapors. Rev Mineral Geochem 76:165–218. https://doi.org/10.2138/rmg.2013.76.6

962 Prather KA, Bertram TH, Grassian VH, et al (2013) Bringing the ocean into the laboratory to probe the
963 chemical complexity of sea spray aerosol. Proc Natl Acad Sci USA 110:7550–7555.
964 https://doi.org/10.1073/pnas.1300262110

965 Rave Y, Jessop D, Moune S (In press) Numerical modelling of the volcanic plume dispersion from the
966 hydrothermal system of La Soufrière de Guadeloupe.

967 Rosas-Carbajal M, Komorowski J-C, Nicollin F, Gibert D (2016) Volcano electrical tomography unveils
968 edifice collapse hazard linked to hydrothermal system structure and dynamics. Sci Rep 6:29899.
969 https://doi.org/10.1038/srep29899

970 Sainlot N. Vlastelic I, Moune S, Rose-Koga EF, Schiavi F, Valade S, Aguilera F (2020) Uptake of gaseous
971 thallium, tellurium, vanadium and molybdenum into anhydrous alum, Lascar volcano fumaroles, Chile.
972 Geochim Cosmochim Ac 275, 64-82. https://doi.org/10.1016/j.gca.2020.02.009

973 Salaün A, Villemant B, Gérard M, et al (2011) Hydrothermal alteration in andesitic volcanoes: Trace
974 element redistribution in active and ancient hydrothermal systems of Guadeloupe (Lesser Antilles). J
975 Geochem Explor 111:59–83. https://doi.org/10.1016/j.gexplo.2011.06.004

976 Scholtysik R, Canil D (2020) Investigation of the effect of Cl on the transport and sublimation of volatile
977 trace metals in volcanic gases using benchtop fumarole experiments. J Volcanol Geoth Res 395:106838.
978 https://doi.org/10.1016/j.jvolgeores.2020.106838

979 Shahidzadeh N, Schut MFL, Desarnaud J, et al (2015) Salt stains from evaporating droplets. Sci Rep
980 5:10335. https://doi.org/10.1038/srep10335

981 Shinohara H (2005) A new technique to estimate volcanic gas composition: plume measurements with a
982 portable multi-sensor system. J Volcanol Geoth Res 143:319–333.
983 https://doi.org/10.1016/j.jvolgeores.2004.12.004

984 Shinozuka Y, Clarke A, Howell S, et al (2004) Sea-salt vertical profiles over the Southern and tropical
985 Pacific oceans: Microphysics, optical properties, spatial variability, and variations with wind speed. J
986 Geophys Res 109:D24201. https://doi.org/10.1029/2004JD004975

987 Sicardi L (1955) Captazione ed analisi chimica dei gas della esalazione solfidrico - solforosa dei vulcani in
988 fase solfatarica. Bull Volcanol 17:107–112. https://doi.org/10.1007/BF02596047

Symonds RB, Gerlach TM, Reed MH (2001) Magmatic gas scrubbing: implications for volcano monitoring. J Volcanol Geotherm Res 108:303–341. https://doi.org/10.1016/S0377-0273(00)00292-4

Symonds RB, Rose WI, Gerlach TM, et al (1990) Evaluation of gases, condensates, and SO2 emissions from Augustine volcano, Alaska: the degassing of a Cl-rich volcanic system. B Volcanol 52:355–374. https://doi.org/10.1007/BF00302048

Symonds RB, Rose WI, Reed MH, et al (1987) Volatilization, transport and sublimation of metallic and non-metallic elements in high temperature gases at Merapi Volcano, Indonesia. Geochim Cosmochim Ac 51:2083–2101. https://doi.org/10.1016/0016-7037(87)90258-4

Tamburello G (2015) Ratiocalc: Software for processing data from multicomponent volcanic gas analyzers. Computers & Geosciences 82:63–67. https://doi.org/10.1016/j.cageo.2015.05.004

Tamburello G, Moune, S., Allard, P., et al (2019) Spatio-Temporal Relationships between Fumarolic Activity, Hydrothermal Fluid Circulation and Geophysical Signals at an Arc Volcano in Degassing Unrest: La Soufrière of Guadeloupe (French West Indies). Geosciences 9:480. https://doi.org/10.3390/geosciences9110480

Taran YA, Bernard A, Gavilanes J-C, et al (2001) Chemistry and mineralogy of high-temperature gas discharges from Colima volcano, Mexico. Implications for magmatic gas–atmosphere interaction. J Volcanol Geoth Res 108:245–264. https://doi.org/10.1016/S0377-0273(00)00289-4

Taran YuA, Hedenquist JW, Korzhinsky MA, et al (1995) Geochemistry of magmatic gases from Kudryavy volcano, Iturup, Kuril Islands. Geochim Cosmochim Ac 59:1749–1761. https://doi.org/10.1016/0016-7037(95)00079-F

Tassi F, Aguilera F, Vaselli O, et al (2009) The magmatic- and hydrothermal-dominated fumarolic system at the Active Crater of Lascar volcano, northern Chile. B Volcanol 71:171–183. https://doi.org/10.1007/s00445-008-0216-z

Tomašek I, Mouri H, Dille A, et al (2022) Naturally occurring potentially toxic elements in groundwater from the volcanic landscape around Mount Meru, Arusha, Tanzania and their potential health hazard. Sci Total Environ 807:150487. https://doi.org/10.1016/j.scitotenv.2021.150487

Varekamp JC (2015) The Chemical Composition and Evolution of Volcanic Lakes. In: Rouwet D, Christenson B, Tassi F, Vandemeulebrouck J (eds) Volcanic Lakes. Springer Berlin Heidelberg, Berlin, Heidelberg, pp 93–123

Global Volcanism Program, 2022. [Database] Volcanoes of the World (v. 5.0.0; 1 Nov 2022). Distributed by Smithsonian Institution, compiled by Venzke, E. https://doi.org/10.5479/si.GVP.VOTW5-2022.5.0

1020 Varrica D, Tamburo E, Dongarrà G, Sposito F (2014) Trace elements in scalp hair of children chronically
1021 exposed to volcanic activity (Mt. Etna, Italy). Sci Total Environ 470–471:117–126.
1022 https://doi.org/10.1016/j.scitotenv.2013.09.058

1023 Vigneri R, Malandrino P, Gianì F, et al (2017) Heavy metals in the volcanic environment and thyroid
1024 cancer. Mol Cell Endocrinol 457:73–80. https://doi.org/10.1016/j.mce.2016.10.027

1025 Villemant B, Komorowski J-C, Dessert C, et al (2014) Evidence for a new shallow magma intrusion at La
1026 Soufrière of Guadeloupe (Lesser Antilles). J Volcanol Geoth Res 285:247–277.
1027 https://doi.org/10.1016/j.jvolgeores.2014.08.002

1028 Wan Y, Wang X, Chou I-M, Li X (2021) Role of sulfate in the transport and enrichment of REE in
1029 hydrothermal systems. Earth Planet Sci Lett 569:117068. https://doi.org/10.1016/j.epsl.2021.117068

1030 Wittmer J, Bobrowski N, Liotta M, et al (2014) Active alkaline traps to determine acidic-gas ratios in
1031 volcanic plumes: Sampling techniques and analytical methods. Geochem Geophys Geosyst 15:2797–2820.
1032 https://doi.org/10.1002/2013GC005133

1033 Xu Y, Dessert C, Losno R (2022) Atmospheric deposition over the Caribbean region: sea salt and Saharan
1034 dust are sources of essential elements on the island of Guadeloupe. J Geophy Res-Atmos

1035 Zelenski M, Kamenetsky V, Taran Y, Kovalskii A (2020) Mineralogy and origin of aerosol from an arc
1036 basaltic eruption: Case study of Tolbachik volcano, Kamchatka. Geochem Geophys Geosyst, 21(2),
1037 e2019GC008802.

1038 Zelenski M, Malik N, Taran Yu (2014) Emissions of trace elements during the 2012–2013 effusive
1039 eruption of Tolbachik volcano, Kamchatka: enrichment factors, partition coefficients and aerosol
1040 contribution. J Volcanol Geoth Res 285:136–149. https://doi.org/10.1016/j.jvolgeores.2014.08.007

1041 Zelenski ME, Fischer TP, de Moor JM, et al (2013) Trace elements in the gas emissions from the Erta Ale
1042 volcano, Afar, Ethiopia. Chem Geol 357:95–116. https://doi.org/10.1016/j.chemgeo.2013.08.022

1043 Zimbelman DR, Rye RO, Breit GN (2005) Origin of secondary sulfate minerals on active andesitic
1044 stratovolcanoes. Chem Geol 215:37–60. https://doi.org/10.1016/j.chemgeo.2004.06.056